NEURAL SYNCHRONY IN SACCADIC TARGET SELECTION IN THE MACAQUE FRONTAL EYE FIELD

By

Jennica M. Sherwood

Thesis

Submitted to the Faculty of the

Graduate School of Vanderbilt University

in partial fulfillment of the requirements

for the degree of

MASTER OF SCIENCE

in

Interdisciplinary Studies: Systems Neuroscience

August, 2006

Nashville, Tennessee

Approved:

Professor Jeffrey D. Schall

Professor Anna Roe

To Mom,

Dad,

Nichole,

Christina,

&

my darling, Pike

in humility, respect, and gratitude

"You cannot revolt: This is two times two equals four! Nature does not ask your permission, she cares nothing of your wishes and whether you like or dislike her laws. You must accept the way Nature is. . . . A wall, this means, is a wall . . . and so on . . . and so on"

Fyodor Dostoevsky, *Notes from the Underground*

ACKNOWLEDGEMENTS

This work would not have been possible without the financial support of the Vanderbilt Brain Institute, the Vanderbilt Vision Research Center, the Center for Cognitive and Integrative Neuroscience, and NIH grants R01 EY08890 and T32 MH064913. I would like to thank Dr. Jeffrey Schall for the opportunity to pursue this project and the resources with which to pursue it, Pierre Pouget for his enthusiasm in continuing this line of research in my absence, and Dr. Lou DeFelice for his support and encouragement throughout my last year of graduate school, which made the difference.

TABLE OF CONTENTS

APPENDIX

LIST OF TABLES

LIST OF FIGURES

CHAPTER I

INTRODUCTION

How visual targets are selected for eye movements is a fundamental neural coding problem for all animals that see with a fovea. The strength of the model of the neuron as a coincidence detector suggests neural synchrony is a plausible, if not intrinsic, part of the cortical code (e.g., Abeles 1982; Softy and Koch 1993; Softky 1995; Konig et al. 1996; Aertsen et al. 1996; Salinas and Sejnowski 2000; Azouz and Gray 2003; Xu et al. 2006). As such, it may play a role in saccadic target selection in the macaque frontal eye field (FEF), a vital node in the visual target selection and saccade production networks (for review, see Schall and Thompson 1999; Schall 2002). Recently, synchronized activity in the gamma frequency range (30 – 60 Hz) among neurons in cortical area V4 has provided evidence for a parallel population search mechanism in visual target selection (Bichot et al. 2005), supporting the theory that synchrony may be a neural mechanism for selective visual attention (Singer and Gray 1995; Usrey and Reid 1999; Engel et al. 2001). Like V4, the frontal eye field (FEF) has visually responsive neurons that participate in the target selection process, combining input from both spatial- and object-oriented visual processing pathways (Schall et al. 1995a) to form an explicit topographic representation of

target identity and location[1] (e.g., Schall and Hanes 1993; Schall et al. 1995b; Thompson et al. 1996; Bichot and Schall 1999; Sato et al. 2001). It is thus plausible that the FEF would make use of neural codes endemic to the cortical areas with which it is densely reciprocally connected, like V4, particularly during concurrent visual processing. As such, synchrony may play a role in the target selection process in FEF.

Variability in spike timing has been observed widely in both sensory and motor domains (e.g., Werner and Mountcastle 1963; Schiller et al. 1976; Vogels et al 1989; Azouz and Gray 1999; Ronacher et al. 2004). While the cortical spike train has been modeled as a Poisson process to capture the variability of the inter-spike interval (ISI) (Perkel et al. 1967; Shadlen and Newsome 1998; Shinomoto and Tsubo 2001; Shinomoto et al. 2005; Luccioli et al. 2006), whether or not there is a signal in the "noise" (variable ISI) has been highly contested (e.g., Softky and Koch 1993; Shadlen and Newsome 1994; Shadlen and Movshon 1999). One influential hypothesis supports the idea that variability in spike timing is an adaptive response to massive convergence of synaptic input onto the single cortical neuron, where "high-input" conditions seem to prohibit the transmission of temporally precise signals beyond chance (Shadlen and Newsome 1994; Shadlen and Newsome 1998)[2]. However, recent studies have

[1] Unlike V4 neurons, FEF neurons show little to no selectivity for individual features of the target such as color or shape (Mohler et al. 1973; Schall 1995a); in the rare instance that they do, it is the result of stimulus-response associations gained through long-term experience with a particular task and stimulus set (demonstrated in macaques after prolonged testing/training, reported in Bichot et al. 1996). Feature-selectivity in FEF is interesting from the viewpoint of cortical plasticity, but it is not an intrinsic property of the neurons prior to experience-dependent change.

[2] More specifically, Shadlen and Newsome (1994, 1998) argue that irregular ISIs arise from the inhibitory PSPs (postsynaptic potentials) required to balance the thousands of excitatory

established the existence of coincidence detection schemes in the cortical neuron *in vivo*, where voltage-gated conductances can adaptively enhance sensitivity to synchronous inputs under high-input conditions, simultaneously decreasing the single neuron's sensitivity to temporally uncorrelated inputs (Azouz and Gray 2000, 2003). Growing evidence for coincidence detection in dendritic spines further supports the relevance of temporally structured signals in neural coding (Coss and Perkel 1985; Yuste and Denk 1995; Zador and Dobrunz 1997; Xu et al. 2006), suggesting a brain engineered for temporal sensitivity at the level of the cell membrane.

This trend extends from the single neuron to fine-scale functional networks, where circuit organization enables the decisive transfer of temporally structured input to postsynaptic neuron firing patterns. Specificity of circuit organization has been shown to induce stereotyped and repeatable synchronous activation in the retinogeniculate and geniculostriate pathways[3] (Alonso et al. 1996; Dan et al. 1998; Usrey et al. 1998; Usrey and Reppas 1999). Additionally, cortical modules, or regions of cortex devoted to topographically and/or functionally circumscribed processes (for review, see Mountcastle 1997), may also be supported by temporally structured activity in sub-networks. For example, Yoshimura et al. (2005) and Yoshimura and Callaway (2005) have shown that fine-scale assemblies of neurons connected within layers 2/3 of striate cortex

---

connections converging onto the single neuron in cortex; without inhibition to balance what they call a "high input regime" of excitatory PSPs, the neuron's firing capacity would be saturated, limiting its dynamic firing range. According to this theory, variable ISI is the adaptive mechanism that allows the regulation of firing rate in the neuron.

[3] Retinogeniculate: from retina to the lateral geniculate nucleus of the dorsal thalamus (LGN); geniculostriate: from LGN to striate (primary visual) cortex, or V1.

(V1) may give rise to the larger functional architecture of V1 columns through synchronous activation from common input from layer IV. This challenges the idea that connections in cortex are inherently probabilistic (e.g., Hellwig et al. 1994; Binzegger et al. 2004) and signals must be averaged over many neurons to improve the neural representation of stimulus properties (Shadlen and Newsome 1994, 1998). Rather, neural representation may arise from sub-networks that explicitly make use of spatially and temporally precise activity.

To investigate a synchronous ensemble code for saccadic target selection in the macaque frontal eye field (FEF), we applied a method of multiple neuron analysis, the gravity algorithm (Gerstein et al. 1985), to simultaneously recorded neurons of a macaque monkey performing color singleton search. The gravity algorithm has been shown to be as efficient as cross-correlation (Moore et al. 1966) in its temporal sensitivity to synchronous cell pairs (Strangman 1997); however, unlike traditional correlation-based methods for the analysis of simultaneously recorded multiple units[4], the gravity method is not limited to representing pair-wise neural interactions alone. Rather, it can represent the coincidence structure of an unlimited number of simultaneously recorded neural spike trains. This is particularly attractive given the feasibility of simultaneous recording from populations of more than 100 neurons at a time (e.g., Wilson and McNaughton 1993).

Temporally-coordinated population codes propose intriguing hypotheses about the neural mechanisms for selective attention, linking millisecond-level

[4] Cross-correlation (Moore et al. 1966) and the joint peri-stimulus time histogram (Aertsen et al. 1989) are popular methods of investigating synchronous pair-wise interactions.

events with higher-order brain functioning. Capacity limits on information processing are a fundamental constraint on most sensory domains, particularly vision (for reviews, see Desimone and Duncan 1995; Kastner and Ungerleider 2000; Moore 2006). As an adaptive mechanism for overcoming capacity limits, attention has been shown to gate and enhance the neural representation of stimulus properties toward meeting behaviorally-relevant goals[5] (e.g., Hsiao et al. 1993; Motter 1993; McAdams and Maunsell 1999; Burton and Sinclair 2000). In the early visual pathway, response synchronization is a mechanism for selective attention, functionally linked to perceptual scene segmentation through orientation tuning and contour grouping in primary visual cortex (Engel et al. 1991; Gray et al. 1992; Aertsen and Arndt 1993; Singer and Gray 1995; Fries et al. 2001a; Roelfsema et al. 2004; Samonds et al. 2004; Samonds and Bonds 2005 Samonds et al. 2006). Synchrony has been further implicated as a mechanism for attention in higher-level processing for color and form in the ventral pathway. Fries et al. (2001) reported the simultaneous enhancement of gamma-range synchrony and reduction of low frequency synchrony (< 17 Nz) among V4 neurons when attention was directed to a target for which the neuron

[5] In a classic study of attention in the object-oriented visual pathway, Moran and Desimone (1985) demonstrated that the locus of attention in a cell's receptive field directly mediated its stimulus-related response, with the magnitude of the effect increasing progressively alongside receptive field size throughout the ventral processing stream. In inferotemporal cortex (IT), where single receptive fields can span the bulk of the contralateral and ipsilateral visual field, cells often failed to respond to the presence of a stimulus in the receptive field when attention was directed outside the receptive field. In other words, representations of unattended stimuli were dramatically suppressed or "filtered" through the attenuation of firing rate. In that study, as in many others, firing rate was the index by which the influence of attention on neural representation was gauged. While there are reasoned arguments for the explicit use of rate-based measures of neural activity, the growing availability and sophistication of multiple-unit recording and analysis open up new vistas for the investigation of neural ensemble interactions (see Brown et al. 2004).

was tuned, as opposed to adjacent V4 neurons activated by distractors. Bichot et al. (2005) extended this result to show a uniform increase in gamma band synchrony among V4 neurons driven by distractors that shared a stimulus property in common with the target. This not only suggests that the locus of attention can enhance neural representation of stimuli through synchrony, but suggests it may bias the representation of stimuli sharing features with the target in the visual search process.

From the cognitive perspective, long-standing theories of visual search have sought to account for how attention is distributed across the visual field in the target selection process. For example, Thompson and Bichot (2005) suggest that target identity is signaled in FEF through the continuous, parallel representation of target and distractors in a topographic map of space; here, target identity is conveyed through a "winner-take-all" selection of the individual location in the topographic map with the peak firing rate. In this case, firing rate is the mechanism by which the neural representation of target identity emerges. However, rate-averaging can mask the temporal structure of spiking activity. For example, Georgopoulos et al. (1988) proposed an influential rate-based vector summation model for the coding of arm direction by neurons in primary motor cortex (M1). Later work by Grammont and Riehle (2003), however, showed that periods of increased synchrony among M1 neurons precede increases in firing rate across large populations of neurons, suggesting a hybrid neural code where synchrony gates rate-based processing. As synchrony has been shown to be a

neural mechanism of selective attention in the somatosensory domain[6] (e.g., Steinmetz et al. 2000), the visual domain (e.g., Fries et al. 2001, Bichot et al. 2005), and has been hypothesized to gate attention in general cortical processing (Niebur et al. 1993; Engel et al. 2001; Niebur 2002), it is plausible that the target selection process may incorporate synchrony to gate or bias visual attention. This opens up the possibility that rate-based evidence has masked the role of synchronous firing in guiding attention toward potentially relevant targets in FEF, motivating this investigation.

[6] For example, Steinmetz et al. (2000) reported an increase in synchrony during task-switching from visual to tactile discrimination in neurons in secondary somatosensory cortex (SII). Synchrony increased by 85% among synchronous pairs when the animal switched from making a difficult visual to a less difficult tactile discrimination, suggesting synchrony subserves not only switching the locus of attention, but reflects modulation of task difficulty.

CHAPTER II

MATERIALS AND METHODS

Experimental design and physiological procedures

Data have previously appeared in Bichot et al. (2001), Sato et al. (2001), Sato et al. (2003), and Schall et al. (2004), where full behavioral training and data acquisition techniques are described[7]. Briefly, spikes were collected from FEF neurons in both hemispheres of monkey F (*Macacca mulatta*) while performing singleton color search for reward. Single units were recorded simultaneously from the rostral bank of the arcuate sulcus with multiple insulated tungsten electrodes (FHC, n ≤ 9) guided through a 1mm spaced grid (Crist et al. 1988) at 1 kHz, sorted offline with a window discriminator. Eye movements were recorded at 250Hz with a scleral search coil surgically implanted prior to recording, analyzed offline for saccadic reaction time. The animal was cared for in compliance with the National Institute of Health's Guide for the Care and Use of Laboratory Animals and the guidelines of the Vanderbilt Animal Care Committee. In total, we included data from 16 ensemble recording sessions for analysis with the gravity algorithm.

Search task

The monkey was seated in a magnetic field for the monitoring of eye position through the implanted search coil. The search array was presented after

[7] Surgical procedures can be found in Schall 1991.

the monkey maintained fixation at a white point in the center of a dark gray screen for approximately 500 ms on each trial. The array consisted of 7 distractors and 1 target aligned iso-eccentrically from the fixation point, scaled from 0.6º of visual angle at 6º eccentricity to 1º of visual angle at 10º eccentricity. The monkey was trained to make a saccade to the color singleton for a juice or auditory reward. Search efficiency was manipulated through target-distractor similarity. Efficient (easy) search trials consisted of a green target among seven red distractors (Comission Internationale de l'Eclairage (CIE) x = 283, y = 612 and CIE x = 655, y = 327, respectively), while inefficient (hard) trials consisted of a yellow-green target (CIE, x = 363, y = 552) among green distractors. Stimuli were matched for luminance (11.1 cd/m^2) and easy and hard trials were interleaved randomly. The behavioral task is shown in Figure 1.

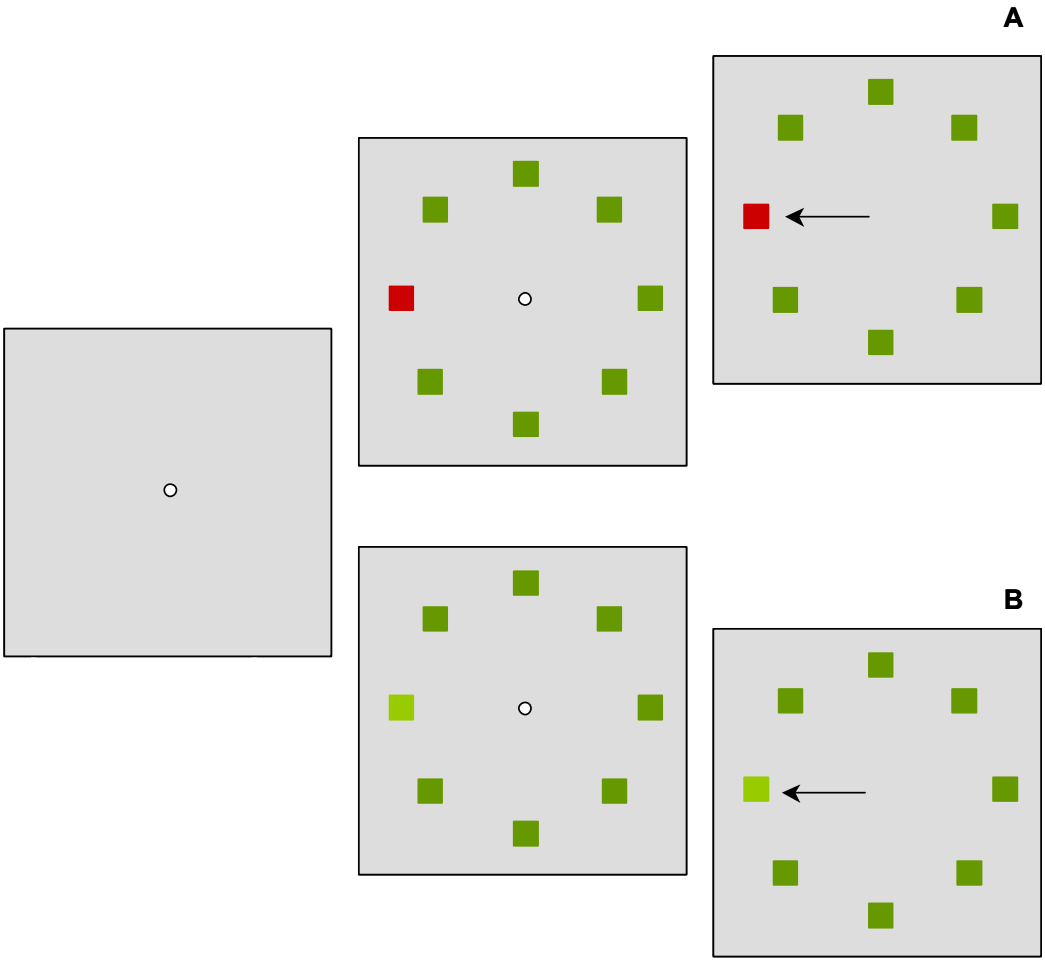

Figure 1. *Behavioral task.* The monkey's task was to shift gaze the color singleton in the array. Gaze was held at fixation point (white circle) until the array was presented. Arrows represent correct saccades. *A,* Efficient search trials ("easy search") required locating a red singleton among green distractors. *B,* Inefficient search trials ("hard search") required locating a yellow/green singleton among green distractors. (Modified from Bichot et al. 2001a).

Gravity algorithm[8]

The gravity algorithm (Gerstein and Aertsen 1985) was applied to the ensemble data collected from each recording session. Broadly, the method treats each of *n* ensemble neurons as points in an *n*-dimensional vector space that move in relation to one another based on the coincidence structure of their simultaneously recorded spike trains. By representing the neurons as points in a common metric space, complex temporal interactions within the ensemble are conveyed through spatial relationships that evolve over the course of the trial period. The distance between neurons at any given millisecond, or the particle-pair distance, is a time-varying index of temporal correlation. In all, each analysis produces one set of particle-pair distances for a single trial period.

More specifically, at the beginning of a trial, all point-particles are arranged equidistantly in the vector space. We selected a value of 100 arbitrarily, but the only relevant constraint in the particles' initial positions is that the number be large enough to prevent them from converging on the same point simultaneously through the duration of the analyzed period. The original configuration for 3 particles in 3 dimensions is shown in Figure 2; in higher dimensions (e.g., as in a 6 neuron ensemble), the initial arrangement can be conceptualized as vertices on a hypercube. This homogeneous spatial ordering deliberately assumes no preferential spike-timing relationships at the outset of analysis (time t = 0 ms).

As each neuron fires, its corresponding particle acquires a charge that decays exponentially; the decay period is specified by the experimenter and can

[8] Programs for implementing and running the gravity algorithm were downloaded from the Mulab webpage and adapted for our own data set and analyses. Original programs can be found at http://mulab.physiol.upenn.edu/programs.html.

be made comparable to the decay period of post-synaptic potential (PSP). We set this parameter to 3 ms such that only spikes with short-lag correlations would be charged over a common interval.

Motion through the vector space is governed by force. More specifically, the force acting along the vector joining any two particles is proportional to the product of the charge on them both; however, unlike electrostatic charges, positive charges attract to reflect coincidence. The sum of all forces acting on a particle is calculated every 1 ms and used in the equation for motion (see Appendix A) to move the particle through the space[9]. The amplitude and

[9]This value can be manipulated to accommodate the analysis of either short-, medium-, or long-lag correlations.

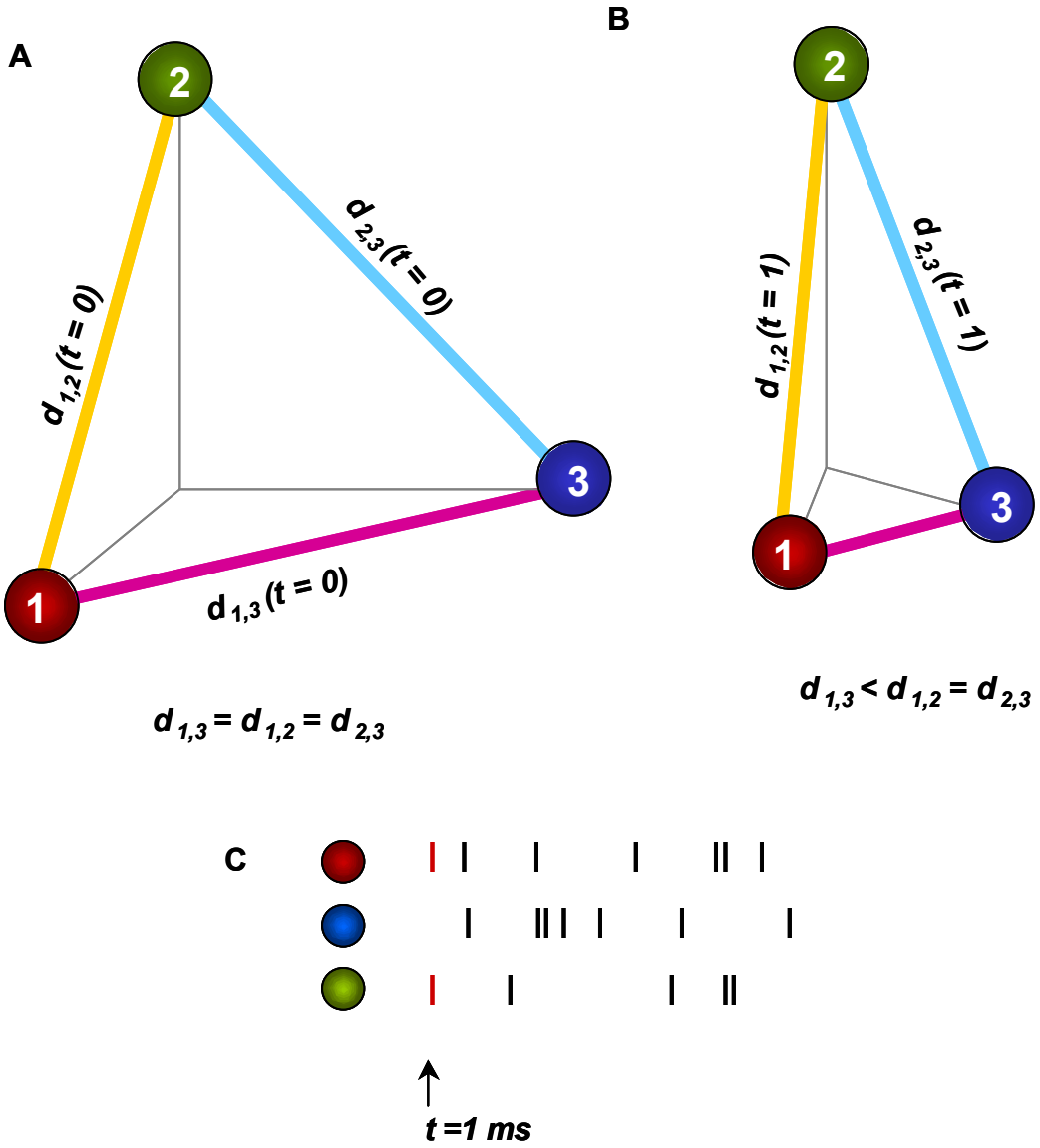

Figure 2. *Spatial configuration of a 3-neuron ensemble. A,* At time *t = 0*, each neuron-particle pair is positioned equidistantly. *B,* At time *t = 1*, neuron 1 and neuron 3 fire simultaneously, indicated in *C,* the cartoon raster plot. Corresponding neuron-particles 1 and 3 acquire a charge that produces an attractive force along the vector between them, drawing them closer. Visual neuron-particle (blue), visuomovement neuron-particle (green), and movement neuron-particle (red) colors combine to signal particle-pair type: visual-visuomovement (cyan), visuomovement-movement (yellow), and visual-movement (magenta).

direction of any given particle's motion, then, is uniquely determined by the interaction of that particle with the entire ensemble.

Force is proportional to velocity (and not acceleration) in the algorithm. This likens the vector space to a viscous medium where particle motility is controlled through a viscosity parameter. Higher viscosity values make movement through the medium more sluggish; lower values speed it up. This is primarily only relevant in relation to the initial configuration of the point-particles. If too low an initial particle-pair distance is paired with too low a viscosity constant, vigorous synchronous activity may cause the particles to converge on one point before the trial period is complete.

The detection of anti-correlation among spike trains

Because the gravity algorithm is explicitly designed to detect synchrony, it is not as sensitive to the detection and representation of anti-correlation among spike trains. This is ultimately due to the fact that motion in the vector space is mediated solely by attractive forces; there is no explicit repulsive force (induced by a repelling charge) integrated into the equation of motion (see Appendix A). Increases in distance between particles, therefore, result when some particles are selectively drawn closer at the exclusion of non-interacting particles. Rapid or noisy movement by one particle away from another may be the result of structured spike-events occurring elsewhere in the ensemble, not necessarily as the result of an inversely correlated relationship between the particle and the

ensemble. With this in mind, we associated increases in particle pair distance with asynchrony, but not its stronger form, anti-correlation.

Recent enhancements to the algorithm

Recent enhancements to the gravity algorithm present an adaptive charge filter for the detection of both short- and long-lag temporal correlations between neurons (Lindsey and Gerstein 2006). In its standard and original form (Gerstein et al. 1985), the charge decay parameter is static throughout the period of analysis; the experimenter selects a short decay constant to detect synchrony on fast timescales, or a longer decay constant to detect longer-lag correlations. The primary enhancement invoked by the dynamic charge filter is a pronounced sensitivity to long-lag correlations, reflected in the increased aggregation of particles-pairs correlated over longer time periods. As we sought to detect synchrony in intervals of 3 ms or less, we did not incorporate recent enhancements to the method and instead used the original form (Gerstein et al. 1985).

The formal details of the algorithm are presented in Appendix A.

Significance testing: Poisson envelope

A certain amount of synchrony can be expected to occur by chance across simultaneously recorded spike trains even if synchrony is not relevant to the neural code under investigation. There is no standard statistical test for the gravity representation, so we developed a method that compares the particle-pair

distances of recorded neurons with particle-pair distances from stochastically generated spike trains, an analogue to the "shift predictor" in the cross-correlogram (e.g. Gerstein and Perkel 1969, 1972). By driving ensemble activity with Poisson processes, we were able generate particle-pair distances from spike trains that had no *a priori* temporal interactions on smaller timescales. This, in turn, provided a time-randomized comparison against which significant synchrony in the real recorded spike trains could be detected. The goal was to provide a set of controls that would form the basis of comparison against which the experimentally derived particle-pair distances could be evaluated for millisecond-level interactions.

Simulating ensemble activity

Given that this study analyzed interactions of cell classes in FEF, we wanted the simulated spike trains to reflect the response properties of the recorded neurons in each ensemble. At the same time, we wanted to introduce the intrinsic stochastic variability in ISI associated with the Poisson process as a control against which to measure temporally precise activity. To accomplish this, we applied a sliding window to each recorded neuron's spike density function (SDF) and sampled the mean firing rate over the window's interval[10]. More specifically, the instantaneous firing rate *A* for a neuron at time *t* was given by the equation describing the neuron's SDF,

[10] The SDF is a smooth representation of the distribution of a neuron's firing rates over time, generated by convolving each action potential in a spike train with an exponential function that has a growth and decay period similar to the post-synaptic potential (PSP).

$$A(t) = (1 - e^{\frac{-t}{\tau_g}})((1 - e^{\frac{-t}{\tau_d}}),$$

where τ_g was a growth parameter set to 1ms and τ_d was a decay parameter set to 10ms. This parameter was selected because it was between the 3 ms decay period used in the gravity algorithm and the 20 ms decay period used in prior measures of target-selection processes in FEF (e.g., Thompson et al. 1996), and it is also a mid-range value for estimates of the membrane time constant for integration of post-synaptic potentials (see Koch et al. 1996).

The firing rates generated by each recorded neuron's SDF were used to drive a rate-modulated Poisson process, where the distribution of events or "spikes" generated by the Poisson process constituted the simulated spike train. More specifically, for any given firing rate λ_k in the k^{th} interval of the trial period, a spike train was produced by defining a Poisson distributed random variable over a *k* ms period:

$$P\{N(t) = m\} = f(m; \lambda_k t) = \frac{e^{-\lambda_k t}(\lambda_k t)^m}{m!},$$

where $N(t)=m$ is the number of events or "spikes" occurring before time t.

In rare instances (< 5.2%), weakly firing neurons with high frequency noise biased the rate parameter used to drive the Poisson process toward the extreme values. In those cases, a 9-pole low-pass butterworth filter was applied to the SDF from which the rate parameters were sampled, passing frequency components of the signal that were one-third or less of the peak value of the

SDF's power spectrum (*MATLAB,* The MathWorks, Inc.)[11]. This served only to reduce the high frequency noise while preserving the underlying distribution of firing rates. See Figure 3.

[11] This particular cutoff frequency for the lowpass filter was selected by trial and error, through eyeballing the improvement of filtered SDFs over original SDFs. More often than not, SDFs requiring filtering at specific locations/conditions had low overall firing rates (fewer spikes to convolve with the exponential kernel and average over time meant more jagged functions).

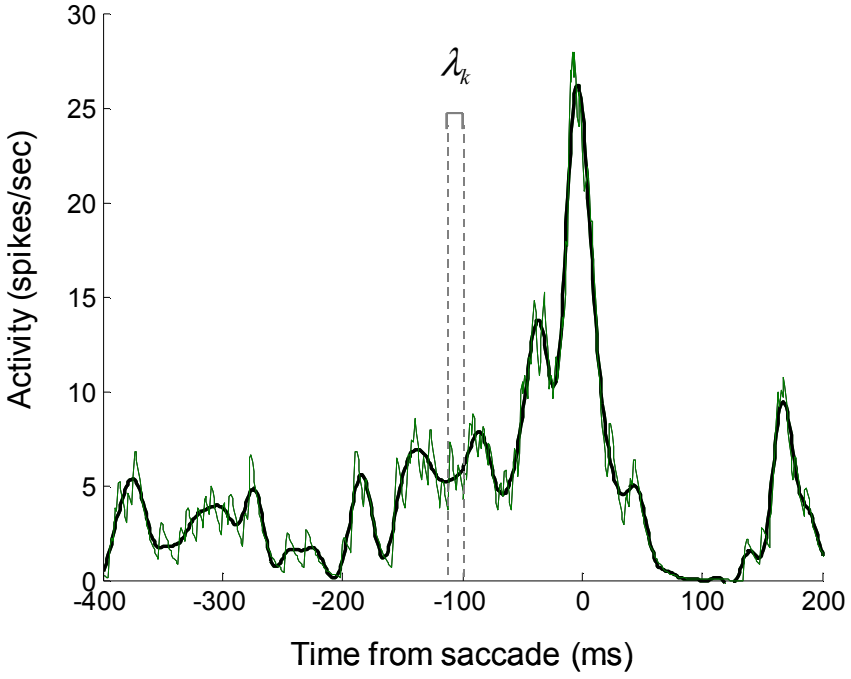

Figure 3. *Filtering for Poisson rate parameters.* High frequency noise in weakly firing neurons were typically at fault in rare cases when the simulation algorithm failed to model the distribution of firing rates given by an SDF. The SDF of a weakly firing visuomovement neuron is shown here (green) alongside its low-pass filtered version (black). Weak spiking activity in an interval like λ_k prompts a jagged SDF where local firing rates are skewed toward extremes. To address the problem, firing rates sampled within any given interval (e.g., λ_k) used to drive simulated spike trains were taken from the filtered SDF (color), which captures the global properties of the interval.

Parameter selection for ensemble simulations

While we aimed to model the distribution of firing rates of each recorded neuron, we did not want to model the distributions *so well* as to make the significance criterion (i.e., the particle-pair distance envelopes generated by the simulated spike trains) too stringent to detect nonrandom synchrony. Too highly controlled a simulation might ultimately result in too great of overlap between real and simulated particle-pair distances, thus contributing to Type II errors, or failure to identify synchronous events as they truly occur. The issue is technically one of timescale. As the sampling bin-size shrinks, the position of individual spikes becomes more relevant than the number of spikes per bin (Rieke et al. 1997). Thus, if we were to cull rate parameters from the original data to drive the simulation every 1 ms, we would essentially produce a concatenation of 600 distinct distributions, each a binary code for "yes" (a spike occurred on average) or "no" (a spike didn't occur on average). The simulated spike trains derived from that set of rate parameters would produce particle-pair distances having near perfect overlap with the original.

To balance the need to limit Type II error while still preserving the underlying distribution of firing rates (reflecting the response properties of each recorded neuron), we chose three different sampling intervals, amounting to three different sets of simulated spike trains. Each interval matched the length over which a firing rate was sampled from the original SDF. This interval, in turn, was also the length of time over which that parameter was used to drive the simulated neuron's activity. In all, we had simulations corresponding to three

sampling interval classes: 10 ms, 15 ms, and 20 ms. Sampling bins greater than 20 ms were excluded because they failed to produce trials that modeled the original distribution of the recorded neuron's firing rates (paired-t test).

Generating significance envelopes

In all, we generated 99 simulated spike trains for each condition appearing in the original data set (i.e., for each neuron by target location by search difficulty by align event). Significance envelopes were generated for the 10, 15, and 20 ms classes. To accomplish this, all simulated spike trains were analyzed with the gravity algorithm using parameters identical to those applied to the original data. Significance values were determined by identifying the extreme maximum and minimum particle-pair distance across the combined trials, parsed into 1 ms bins. For example, for any neuron *n* in ensemble *E*, the upper significance boundary value ($S_{E,n,\,max}$) across all particle-pair distances $p_1 \ldots p_{99}$ at millisecond t_k was:

$$S_{E,n,\,max}\,(t_k) = max(p_1(t_k), \ldots, p_{99}(t_k)).$$

Each numerical subscript corresponds to trial number. These values combined to create a series of upper and lower bounds for the trial period, $S_{E,n,\,max}\,(t_1, \ldots, t_{600})$ and $S_{E,n,\,min}\,(t_1, \ldots, t_{600})$, respectively.

Original data were then paired with significance envelopes and compared at each 1 ms interval. Particle-pair distance excursions outside the envelope (exceeding the maximum value or falling below minimum value for the 1 ms

interval) were considered unlikely to occur by chance with 99% confidence. In other words, by finding the limit values of 99 time-randomized particle-pair distances for each condition, we established a measure wherein, 99 times out of 100, it would be unlikely for a particle-pair distance to make an excursion outside the significance envelope if it were *not* synchronous beyond chance. Instances of significant synchrony were registered in a histogram that spanned the trial period for each particle-pair type across all trials.

Cumulative density estimates of synchrony across the trial period

To examine the cumulative distribution of synchronous events across the trial period, we computed a Kaplan-Meier estimate for each probability density function of synchronous spikes given by a normalized significance histogram. Formally, the probability *S* that a synchronous event *k* "survived" or occurred beyond time *t* throughout the trial period was given by

$$S(t) = 1 - F(t),$$

where *F* is the probability a synchronous event failed to "survive" or did not occur beyond time *t*.

For *N* total synchronous spikes, then, we let $t_1 \leq ... \leq t_k \leq ... t_N$ be the observed times *t* at which *k* spikes "failed to survive" beyond *t* in the significance histogram. This means that for each time t_k, there was both a number of surviving synchronous events, n_k, and a number of non-surviving synchronous events, f_k, in the significance histogram. The Kaplan-Meier estimate of the

cumulative density of spikes across the trial period at time *t* was thus given by the survival function $\hat{S}$, where

$$\hat{S}(t) = \prod_{t_k \le t} \frac{n_k - f_k}{n_k}$$

($\hat{S}$ is an estimate of the continuous function S).

We then calculated the period of the greatest growth in synchronous activity in the trial period by computing the numerical derivative of the survival function $\hat{S}$ and finding its global maximum, which matched the global maximum of the probability density function provided by the normalized synchrony histograms.

Our predictions for synchronous activity were based on cell-class interaction, receptive field organization of neurons pairs, and the influence of search efficiency.

Analysis by physiological cell class

Because the gravity algorithm measures distance between neuron pairs, we organized the analysis according to whether the pairs came from common or distinct physiologically defined cell-classes. This required the classification of the activity of each recorded neuron in relation to trial events based on previously established cell response properties (given in Bruce and Goldberg 1985; Schall 1991; Schall et al. 1995a).

Briefly, a mixed population of visual, movement, and visuomovement neurons participate in the sensorimotor transformation from target selection to

saccade production in FEF (Bruce and Goldberg 1985; Schall et al. 1995b). The firing rate of visually responsive neurons has been shown to represent target-related information (Schall and Hanes 1993; Schall et al. 1995b; Thompson et al. 1996; Bichot and Schall 1999; Bichot et al. 2001a), while motor neurons increase firing rate in association with preparation and execution of a saccade into their response fields (Bruce and Goldberg 1985; Schall 1991; Hanes et al. 1995; Hanes and Schall 1996; Hanes et al. 1998). Visuomovement neurons are active in both sensory and motor stages of processing (Bruce and Goldberg 1985; Schall et al. 1995b), and the evolution of their activity over the course of the trial period, measured in firing rate, reliably distinguishes target from distractors. Signal-processing techniques have been adapted from the measurement of psychophysical thresholds to estimate the time at which “neural” threshold is reached in visuomovement neurons for the discrimination of a target, or target discrimination time (TDT) (Thompson et al. 1996; see Britten et al. 1992 for an outline of the original “neuron-anti-neuron” method). TDT has been hypothesized as the time at which an explicit representation of target identity and location is formed in the neuron (see Thompson et al. 1996; Sato et al. 2001). We selected the gravity method for analysis by physiological cell-class based on its previous success in detecting synchronous cell assemblies involved in the motor control and regulation of breathing via respiratory-related nuclei in the medulla (Lindsey et al. 1992a, 1992b, 1994, 1997; Arata et al. 2000; Morris et al. 2000, 2001). We predicted differences in the temporal interactions of the neurons based on the particular overlap of physiological classes described by each union. See Figure 4

for representative spike density profiles of visual, visuomovement, and movement neurons from the analysis.

Cell-class pairs were described as homogeneous or heterogeneous. Homogeneous cell-classes were divided by visual-visual, visuomovement-visuomovement, and movement-movement neuron pairings. Heterogeneous cell-classes were divided by visual-visuomovement, visuomovement-movement, and visual-movement neuron pairings.

Analysis by receptive field interaction

We also characterized the receptive field organization of ensemble neurons in relation to target location. The target was classified according to its appearance in one of the following locations: (i) In the overlap of the pair's receptive fields (overlapping condition), (ii) in one neuron's receptive field, directly adjacent to the other neuron's receptive field (adjacent condition), (iii) in one neuron's receptive field but neither adjacent to nor overlapping with the other neuron's receptive field (in only one receptive field condition), or (iv) outside both neuron's receptive fields (neutral condition). See Figure 5 for an illustration of search arrays in relation to receptive field interaction.

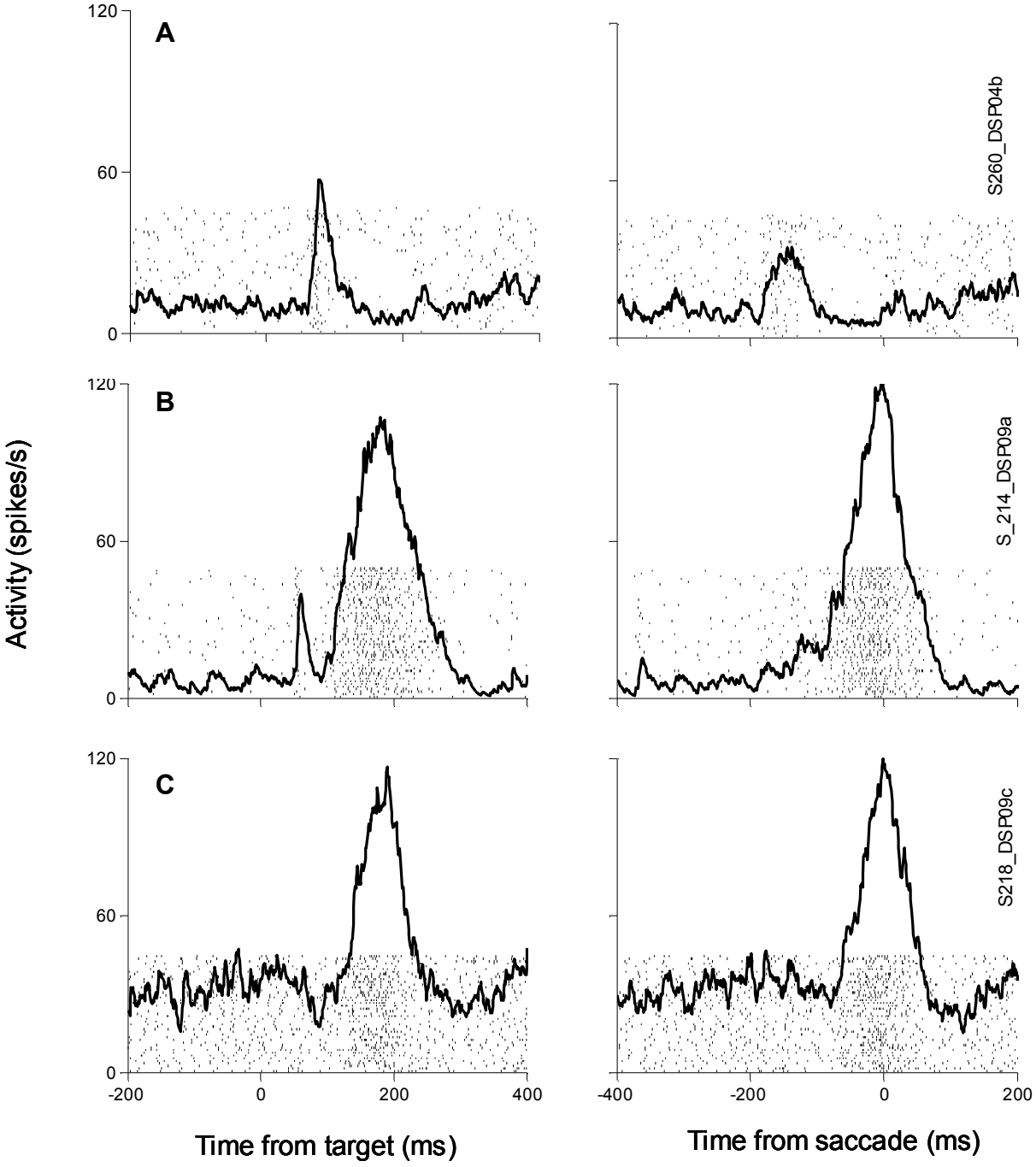

Figure 4. *Cell classes.* Spike density functions (SDFs) for frontal eye field (FEF) neurons during visual search. Vertical tickmarks represent neuronal discharge in the raster displays, aligned on target presentation in the left panel and saccade initiation in the right panel. *A,* Visual neuron. Transient visually-related activity after target presentation, with no selective activity around the time of saccade. *B,* Visuomovement neuron. Phasic visually-related activity after target presentation, followed by movement-related activity around the time of saccade. *C.* Movement neuron. No visually-related activity following target presentation, but strong movement-related activity near the time of saccade.

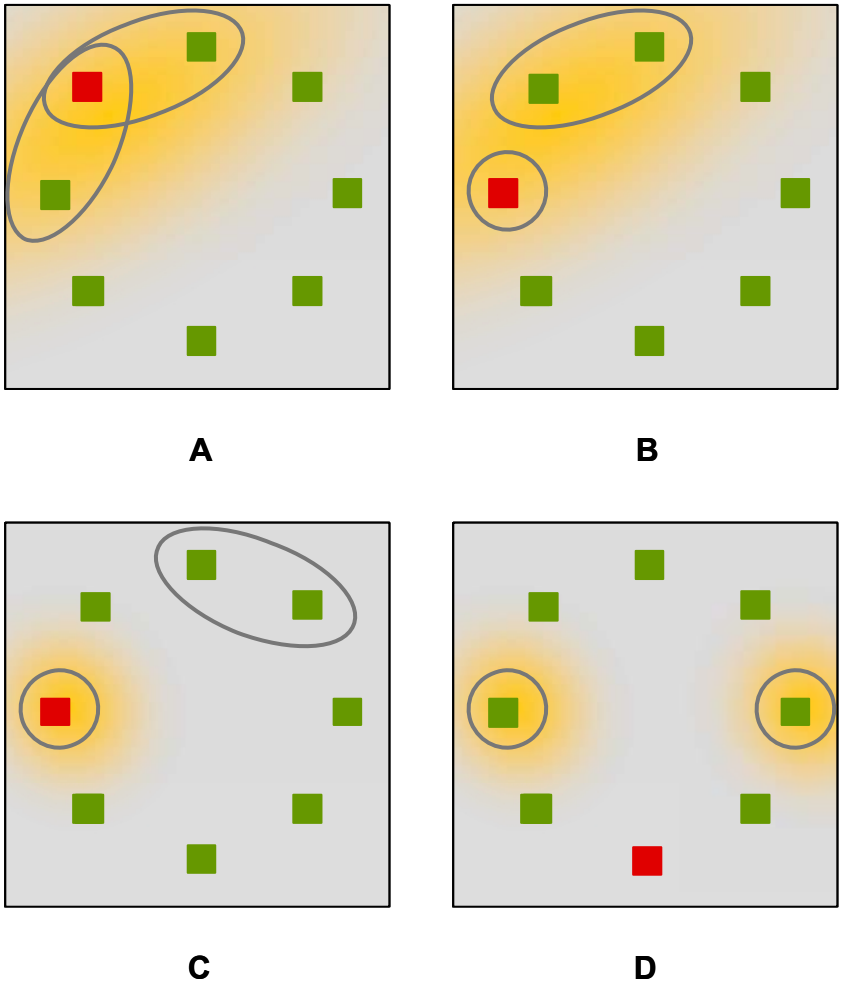

Figure 5. *Receptive field organization.* Particle-pair distances were classified according to the interaction of the color singleton with the cell-pair's receptive fields. *A,* Overlapping condition. The target appears in the overlap of the receptive fields. *B,* Adjacent condition. The target appears in one neuron's receptive field, adjacent to the other's. *C,* Target in only one receptive field condition. The target appears in one neuron's receptive field but is neither overlapping with nor adjacent to the other's. *D,* Neutral condition. The target appears in neither neuron's receptive field.

Analysis by search efficiency

The manipulation of target-distractor similarity has been used extensively to try to dissociate serial from parallel stages of visual processing. Parallel search models were developed in part to explain the discrepancy in mean reaction time between efficient and inefficient search (for review, see Wolfe and Horowitz 2004). During more effortful search, the serial focus of attention across the visual scene has been proposed to account for saccade latencies which are longer than those in "popout" search, where processing has been hypothesized to occur through the parallel encoding of bottom-up feature salience (Treisman and Gelade 1980, Wolfe et al. 1989; Duncan and Humphreys 1989; Wolfe et al. 1994; Treisman and Sato 1990). While the neural estimate of TDT when target-distractor similarity is high is longer in FEF than when target-distractor similarity is low (Sato et al. 2001), why this is so is unclear from a neural coding perspective. To test the hypothesis that synchrony is modulated by target-distractor similarity, we analyzed particle-pair distances according to whether the trial was efficient (red color singleton among green distractors) or inefficient (yellow-green color singleton among green distractors).

CHAPTER III

RESULTS

Behavioral data

Sample particle distance results for a single trial are given in Figure 6, illustrating the output of the analysis in relation to raw ensemble activity and task conditions. Particle-pair distances from 6,024 efficient search trials and 4,734 inefficient search trials contributed to these results. We included only correct trials in the analysis, so the discrepancy in trial number between efficient and inefficient conditions reflects the natural attenuation of performance accuracy in inefficient search. The lag between mean latencies for efficient versus inefficient processing further demonstrates a performance difference; mean saccadic latency between efficient and inefficient trials was significantly different, at 197 ms and 246 ms respectively (t-test, $p < 0.05$). The range of saccade latencies spanned 48 to 1718 ms in efficient search and 119 to 3652 ms in inefficient search.

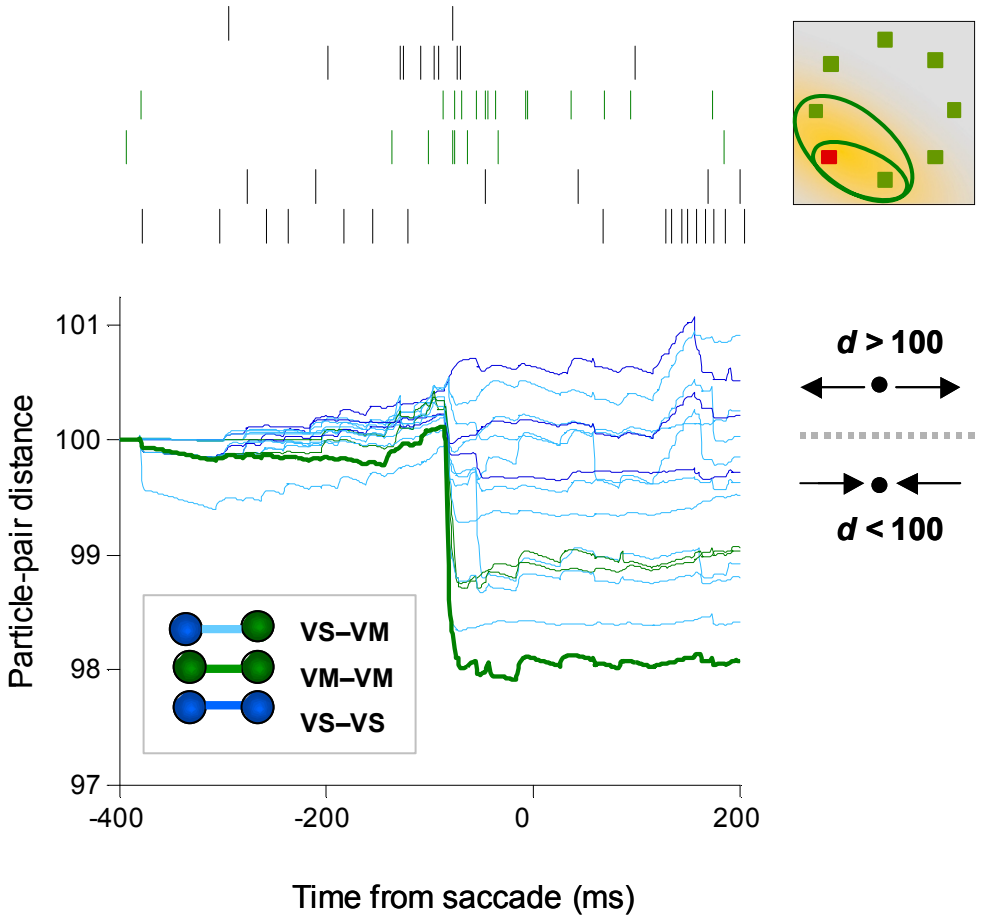

Figure 6. *Particle-pair distances for a single trial.* Particle-pair distances from a 6 neuron ensemble during efficient search. Distance trajectories are color coded by the cell-class interaction of each neuron pair, with this ensemble containing visual (VS) and visuomovement (VM) neurons only. Note that at the beginning of each trial, all distances originate at 100, reflecting the initial positions of the neurons (100 units apart) in the 6-dimensional vector space. As the trial evolves, distance trajectories either exceed or drop below the initial baseline value of 100; distances greater > 100) reflect asynchrony, while distances less than 100 (d < 100) reflect synchrony. The greatest drop in distance between particle pairs occurs approximately 80 ms prior to saccade initiation, reflecting synchrony in the raster plot (located above the distance graph). Each row in the raster plot corresponds to one neuron's spiking activity 400 ms prior to 200 ms after saccade initiation. The receptive field organization of the bold VM-VM pair reaching minimum distance within the ensemble is illustrated in the cartoon.

Distribution of neurons pair types

The distribution of cell types and neuron pairs included in the analysis is presented in Table 1. The majority of the cells were visuomovement (66.6%). Visuomovement-visuomovement neurons pairs were the largest neurons pair type in the analysis (forming slightly less than half of all particle-pair types, 45.1%).

Table 1. *Cell and particle-pair types.*

Type	*n*	*%*
Cell type		
Visual	14	18.7
Visuomovement	49	66.6
Movement	14	14.7
Total cell type	75	100.0
Neuron-pair type		
Visual-visual	5	3.3
Visuomovement-visuomovement	69	45.1
Movement-movement	11	7.2
Visual-visuomovement	37	24.2
Visual-movement	4	2.6
Visuomovement-movement	27	17.6
Total particle-pair types	153	100.0

Simulation Accuracy

The accuracy of the simulated spike trains used to generate the significance envelopes was evaluated by performing a paired-t test of significance on the SDFs generated by recorded versus simulated neurons in each ensemble. The test compared mean instantaneous firing rates for both groups at the 1 ms interval across the full trial period. Failure to reject the groups as significantly different implied a successful simulation. Simulation accuracy for all three Poisson sampling intervals (Δt_λ = 10, 15, and 20 ms) is reported in Table 2. Note that acceptance at higher *p* values required greater simulation accuracy, given that each simulation aimed to achieve no significant difference between group means[12]. Figure 6 plots SDFs from recorded neurons alongside corresponding SDFs produced by the simulation.

Table 2. *Simulation accuracy.* Percentages reflect simulation success rates, or the average number of simulated spike trains producing identically distributed firing rates (SDFs) to recorded neurons. The length of the interval over which the Poisson rate parameter was sampled and used to generate a spike train of the same length is given by Δt_λ.

	Identically distributed firing rates (%)			
Sampling interval	*p* < .01		*p* < .05	
Δt_λ	easy	hard	easy	hard
10 ms	88.2	91.1	79.3	82.9
15 ms	88.2	91.0	79.1	81.7
20 ms	87.6	90.0	78.4	79.1

[12] That is, failure to reject the null at *p* < .05 required more correspondence between means than failure to reject at the *p* < .01 significance level.

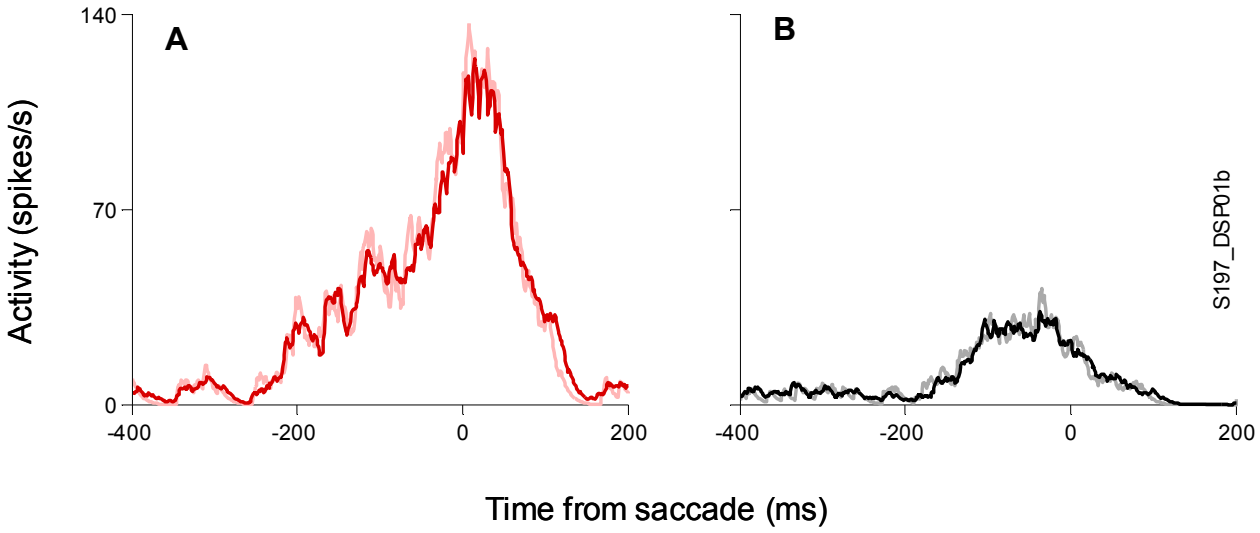

Figure 6. *Simulated versus recorded activity.* Spike density functions (SDFs) generated by simulated and recorded spike trains are plotted together, aligned on saccade. *A,* SDF for visuomovement neuron (pink) and corresponding simulation (red) when saccades was made into the neuron's response field (sampling interval Δt_λ= 10 ms). *B,* SDF for the same neuron (gray) and corresponding simulation (black) when saccades were made to a target outside the neuron's response field.

Sensitivity of significance envelopes in detecting correlation

In order to select the significance measure most sensitive to temporally correlated activity, we measured the performance of each class of significance envelope (10, 15, and 20 ms) in detecting artificial synchrony embedded into recorded ensemble activity. We wanted to identify the class of significance envelope that would detect temporally-precise relationships between as little as two neurons, even when embedded in an otherwise uncorrelated ("noisy") ensemble. To accomplish this, we imposed structured synchronous relationships on randomly selected neurons pairs within each ensemble by devising a "source" and "recipient" spike replacement technique.

Ten percent of the originally recorded trials were randomly selected across all sessions. For each randomly selected trial, two neurons were selected (again, randomly) for correlation and designated either a "source" or "recipient." We tested two levels of synchrony. In the first condition, all source and recipient pair types were perfectly correlated; that is, the source neuron's entire spike train was copied and embedded into the recipient neuron's spike train. Firing rates were conserved to reflect the endogenous properties of the neurons, however, so for each set of *j* spikes copied from the source neuron's spike train, *j* randomly selected spikes were simultaneously removed from the recipient neuron's spike train. See Figure 7 for an illustration of the sampling and replacement technique.

In the second condition, source-recipient synchrony was scaled to reflect the likelihood of correlation based on the response properties of each neuron's physiological cell-class. In this scaled condition, homogeneous neurons pair

types were more strongly correlated than heterogeneous neurons pair types, with a standard correlation of 0.8. Visual-visuomovement and visuomovement-movement pairs were each assigned a 0.6 spike train correlation, while visual-movement pairs, the least likely to have spikes naturally overlap during the trial period, had 0.4 correlation. The source-recipient correlation technique increased synchronous spikes in the selected neurons' spike trains by a factor of 2.6 in the perfect correlation condition and 1.9 in the scaled correlation condition.

The artificially correlated spiking-activity was then analyzed by the gravity algorithm and tested for significance using each envelope class. The sensitivity of each envelope class was defined as the product of the number of trials on which at least one significant event was registered and the number of significant events registered per trial. The 10 ms class, corresponding to significance envelopes generated by spike trains from Poisson processes modulated every 10 ms, demonstrated the best performance. See Table 3 for a summary of envelope sensitivity. Appendix B contains comprehensive results organized by source-recipient pair.

All envelope classes detected the perfectly correlated synchronous condition better than the scaled condition, which we would expect if the envelopes were sensitive not only to the presence or absence of synchrony, but its presence or absence in degrees. Due to the fact that we randomly selected neurons in which to induce correlation, we could not guarantee robust firing rates for every source-recipient pair. This accounts for the less than perfect detection of synchronous events by all envelope classes in the perfect correlation condition

(performance ranged from 80.4% to 85.9%). For example, if the source-recipient pair both had particularly low firing rates, even perfectly correlated spike trains may fail to be detected amidst an otherwise active ensemble, given that particle motion is governed by the sum of all neuron-particle forces in the vector space, not pair-wise force between source and recipient alone.

Figure 8 compares the particle-pair distances for a recorded ensemble alongside distances after scaled- and perfectly-correlated spikes are embedded into the ensemble.

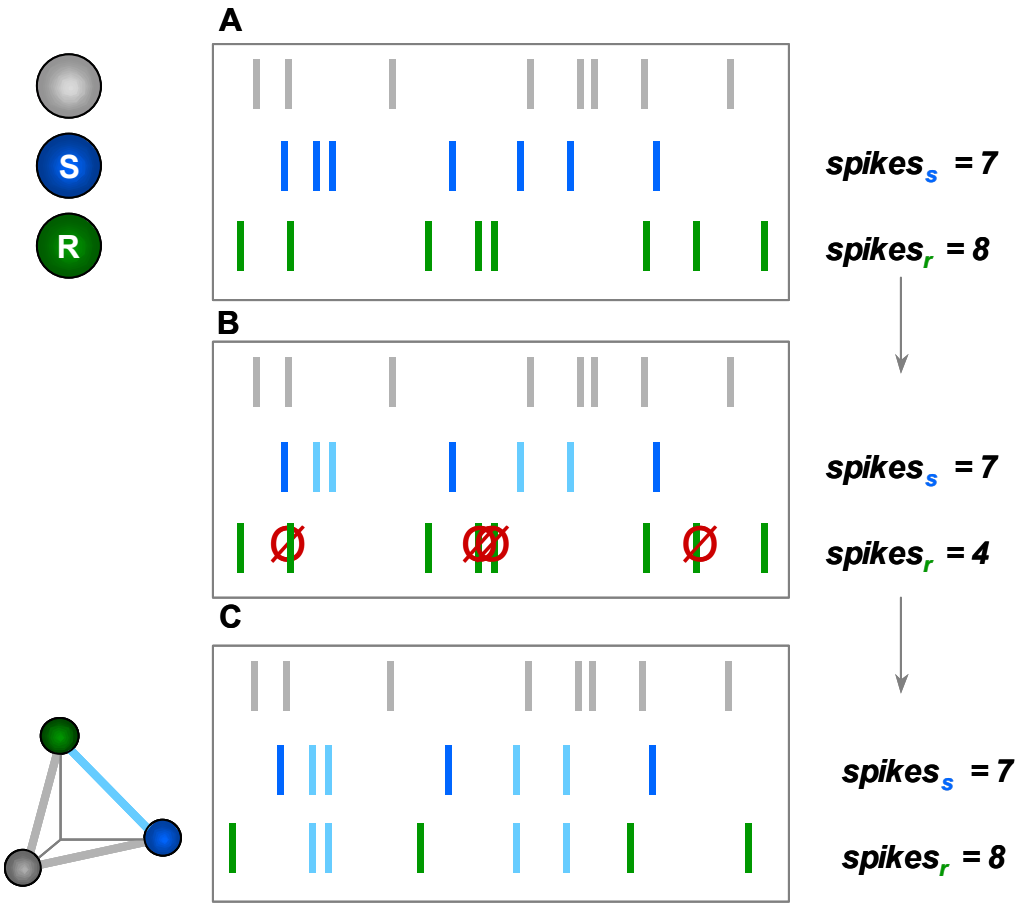

Figure 7. *Inducing artificial temporal correlation.* Synchrony was embedded into simulated spike trains to induce artificial temporal correlation, illustrated here. *A,* Sample spike trains associated with the ensemble's visual neuron (blue) and a visuomovement neuron (green) are randomly selected as a source-recipient pair. The unselected neuron's spike train is not modified in any way. *B,* A fraction of spikes from the source neuron's spike train (~0.6) is selected (cyan) for replication in the recipient neuron's spike train. The same fraction of the recipient neuron's spikes is selected (gray) for deletion from the recipient neuron's spike train. *C,* The randomly selected spikes are embedded in the recipient neuron's spike train. Newly correlated spikes (cyan) are matched in time. Note that firing rate is conserved in the sampling and replacement process.

Table 3. *Significance envelope performance by millisecond-level class.* Percentage of trials on which artificial synchrony imposed on particle-pairs was detected from background ensemble firing. The 10 ms envelope class was used for the set of significance class criterion in the analysis.

	Significant trials (%)	Significant ms/trial (ms)	Scaled product (ms)
PERFECT CORRELATION			
10 ms	83.3	330	275
15 ms	85.9	305	254
20 ms	80.4	298	240
SCALED CORRELATION			
10 ms	72.5	287	208
15 ms	73.9	268	198
20 ms	69.8	262	183

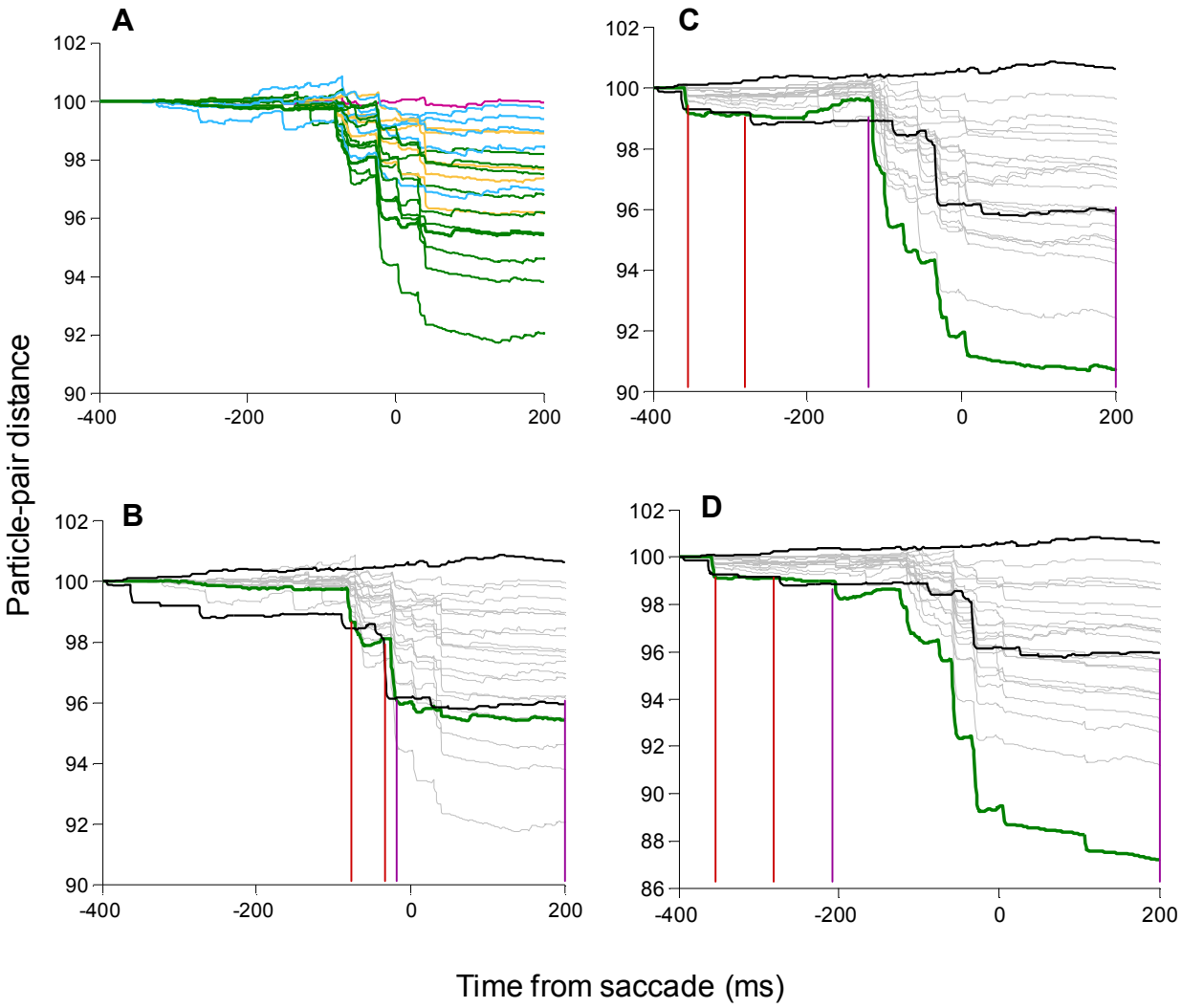

Figure 8. *Particle-pair distances after embedded synchrony.* The sensitivity of the significance envelope to the degree of spike correlation is illustrated. *A,* Recorded ensemble: Particle-pair distances from a 7-neuron ensemble of visual, visuomovement, and movement neurons are plotted. Visuomovement-visuomovement pairs (VM-VM) are in green, visuomovement-movement (VM-MV) pairs are in yellow, visual-visuomovement (VS-VM) pairs are in cyan, and one visual-movement (VS-MV) is in magenta. Note the coarse segregation of synchrony by cell-pair type, with synchrony increasing: VS-MV < VS-VM < VM-MV < VM-VM. *B,* Recorded ensemble: The particle-pair with the greatest synchrony (a VM-VM pair) is in bold, alongside the significance envelope generated for that pair and receptive field condition (overlapping). The first period of significant synchrony is isolated in red, followed by a second period isolated in purple. *C,* Scaled correlation: Particle-pair distances following scaled correlation between the spike trains for the bold VM-VM pair. Note the earlier onset of the first synchronous period (red) and the longer duration of the second synchronous period (purple). *D,* Perfect correlation: Particle-pair distances following perfect correlation for the bold VM-VM pair. Note that the duration of the second synchronous period is longer than in the scaled-correlation condition.

Summary of synchronous and asynchronous activity

The overall percentage of trials with significant synchrony was 6.9%, while the overall percentage of trials with significant asynchrony was 14.0%. There were no significant differences in mean synchrony by receptive field organization or search efficiency (paired t-test, $p = 0.05$). Similarly, there were no significant differences in mean asynchrony by receptive field organization or search efficiency (paired t-test, $p = 0.05$). See Tables 3 and 4 for detailed results by cell-class interaction, search efficiency, and receptive field organization.

There are trends that are worth nothing, nonetheless, in the distribution of synchrony across the search efficiency, cell-class interactions, and receptive field organization conditions. In the synchronous condition, neuron pairs with overlapping and adjacent receptive fields exhibited more synchrony, as a rule, than the neutral and singleton receptive field (target appearing in only one neuron's receptive field) conditions. Inefficient search trials for neurons with overlapping receptive fields were more synchronous than any other group, occurring on an average of 10.1% of trials. There was no particular trend differentiating groups with minimum synchrony values. The greatest amount of asynchrony occurred in inefficient search trials in neurons in the neutral receptive field condition, occurring on 14.9% of all trials. The least amount of asynchrony was for efficient search trials in neurons with overlapping fields.

Maximum synchrony in relation to TDT

We calculated the points of maximum growth in synchrony by finding the global maximum of the probability density function for visual-visual, visual-visuomovement, and visuomovement-visuomovement neuron pairs across the trial period and compared them to previously collected TDT estimates. There appeared to be no systematic relationship between periods of maximum growth in synchrony and TDT by cell-class interaction, receptive field interaction, or search efficiency (Welch's t-test).

Cumulative density of synchrony

The cumulative density of synchrony in relation to target presentation and saccade initiation proved complex and trends were difficult to identify. The most salient result was the marked lack of temporal correlation in the visuomovement-visuomovement pairs in relation to target-distractor similarity, which we would expect to see if our prediction for synchrony as a mechanism for biasing potential target locations were substantiated. Moreover, the lack of significant synchrony between movement-movement pairs prior to saccade initiation suggests synchrony may not be a mechanism for gating broader population responses. The cumulative density results require more careful interpretation for cleaner division and organization of results. See Appendix C for full cumulative density results.

Table 4. *Percentage of total trials with significant synchrony.* Columns: Neuron-pair receptive field organization in relation to target. Entries with one asterisk had significant synchrony for at least 10 ms. per trial on at least 10% of all trials. Entries with two asterisks had significant synchrony for at least 20 ms. per trial on at least 10% of all trials.

	Trials with significant synchrony (%)				
	OVERLAPPING	ADJACENT	IN ONE CELL'S RF ONLY	NEUTRAL	
EFFICIENT SEARCH					
Neuron-pair type					AVG
Visual-Visual	7.4	4.5	2.4	1.7	4.0
Visuomovement-Visuomovement	12.3*	11.0	7.5	10.2	10.3
Movement-Movement	3.5	6.2	4.0	3.8	4.4
Visual-Visuomovement	5.9	5.8	5.1	5.4	5.6
Visuomovement-Movement	10.2	8.7	4.7	6.3	6.3
Visual-Movement	6.6	5.7	7.9	5.1	7.5
AVG	7.7	7.0	5.3	5.4	6.4
INEFFICIENT SEARCH					
Neuron-pair type					
Visual-Visual	14.1**	5.3	2.8	2.3	6.1
Visuomovement-Visuomovement	13.8**	12.3*	8.2	10.9	11.3
Movement-Movement	13.4*	7.2	6.0	5.9	8.1
Visual-Visuomovement	4.6	6.3	6.0	5.6	5.6
Visuomovement-Movement	10.2	10.0	7.0	6.1	8.3
Visual-Movement	4.7	4.0	7.4	4.6	5.2
AVG	10.1	7.5	6.2	5.9	7.4
GRAND AVG	8.9	7.3	5.8	5.7	6.9

Table 5. *Percentage of total trials with significant asynchrony.* Columns: Neuron-pair receptive field organization in relation to target. Entries with one asterisk had significant asynchrony for at least 10 ms. per trial on at least 10% of all trials. Entries with two asterisks had significant asynchrony for at least 20 ms. per trial on at least 10% of all trials.

	Trials with significant asynchrony (%)				
	OVERLAPPING	ADJACENT	IN ONE CELL'S RF ONLY	NEUTRAL	
EFFICIENT SEARCH Neuron-pair type					AVG
Visual-Visual	9.5	14.7	15.9	16.0	14.0
Visuomovement-Visuomovement	14.7	15.2	14.7	14.8	14.9
Movement-Movement	7.4	10.2	9.8	7.8	8.8
Visual-Visuomovement	15.3	15.5	12.3	15.6	14.7
Visuomovement-Movement	14.8	13.2	13.2	10.8	13.0
Visual-Movement	16.6	16.5	12.1	13.1	14.6
AVG	11.8	14.2	13.0	13.0	13.3
INEFFICIENT SEARCH Neuron-pair type					
Visual-Visual	8.7	14.9	19.9**	15.7	14.8
Visuomovement-Visuomovement	15.7	16.2	17.8	16.9	16.7
Movement-Movement	12.8	9.5	11.9	12.2	11.6
Visual-Visuomovement	16.3	15.3	15.3	16.0	15.7
Visuomovement-Movement	15.5	15.2	14.5	13.1	14.6
Visual-Movement	16.6**	15.0*	9.5	15.4	14.1
AVG	14.3	14.4	14.8	14.9	14.6
GRAND AVG	13.0	14.3	13.9	14.0	14.0

Discussion

Determining the functional interaction of cell classes in FEF is made especially complex by the FEF's location in a densely interconnected network. While the notion of a "hierarchy" of visual processing may be controversial and even obsolete (see Felleman & Van Essen 1991, Van Essen et al. 1992; Hochstein & Ahissar 2002), the FEF is nonetheless remarkably distinguished in the breadth of inputs it receives from more than 20 cortical areas, which combine to project feature-, memory-, and goal- related information to FEF (see Schall et al. 1995a; Thompson & Bichot 2005). The interaction of the functionally heterogeneous cell classes in FEF has yet to be fully characterized; unfortunately, the interpretation of the results of the gravity analysis proved ambiguous.

To test the general prediction of synchrony as a mechanism of selective attention, we predicted synchrony would increase among homogeneous visuomovement neurons pairs with the level of target-distractor similarity, biasing visual attention toward cells with receptive fields stimuli that share features with the target. Moreover, we predicted an increase in synchrony among homogeneous movement neurons pairs in trials when the target appeared in overlapping response fields, biasing attention toward topographic locations that signal the correct amplitude and direction of gaze shift. We also predicted an increase in transient synchrony following the onset of the target and a stereotyped afferent delay associated with the onset of visual activity in FEF (see

Pouget et al. 2005). Finally, we predicted homogeneous cell pairs (e.g., visual-visual, visuomovement-visuomovement, movement-movement) would show more synchronous activity at or around the time of their response-related events. None of these predictions yielded easily to interpretation with the given results.

Observations about surround-related suppression were considered in receptive field analysis. Schall et al. (1995b) reported a correspondence between the attenuation of activity (or "response suppression") of a neuron with a distractor appearing in its receptive field and the proximity of the target, which may give rise to more asynchrony among visuomovement-visuomovement pairs in the adjacent receptive field condition (where the target appears in the receptive field of one neuron but is adjacent to the other), alongside more synchrony in the overlapping receptive field condition. Preliminary results did find synchrony in the overlapping receptive field condition, and moderate asynchrony in the adjacent receptive field condition, but full interpretation of the particular quantification of the degree of synchrony (percent of trials on which synchrony occurred) will require comparing the outcome of correct versus incorrect trials. Analysis of incorrect trials will provide a basis of comparison against which to scale the functional impact of the degrees of synchrony reported.

At this stage, more careful interpretation of results will be required to draw meaningful conclusions about the effect of synchrony on selective visual attention in saccadic target selection. Appendix D contains a table of predictions to guide subsequent interpretation of these results.

APPENDIX A

FORMAL CHARACTERIZATION OF GRAVITY METHOD

Each ensemble of *n* recorded neurons was characterized as a point-particle in an *n*-dimensional vector space. The initial positions of the particles described orthogonal basis vectors for the space, with orthogonality conferring the property of equidistance between any two points. Any *n*-neuron ensemble described by the vectors $\vec{x_1}, \vec{x_2}, ..., \vec{x_n}$ assumed the normalized initial positions

$$\left\|\vec{x_1}\right\| = (\frac{\sqrt{2}}{2}, 0, 0, ..., 0)$$

$$\left\|\vec{x_2}\right\| = (0, \frac{\sqrt{2}}{2}, 0, ..., 0)$$

$$\left\|\vec{x_3}\right\| = (0, 0, \frac{\sqrt{2}}{2}, ..., 0)$$

...

$$\left\|\vec{x_n}\right\| = (0, 0, 0, ..., \frac{\sqrt{2}}{2})$$

such that the distance between any two particles $\vec{x_j}$ and $\vec{x_n}$ was

$$\left\|\vec{x_j} - \vec{x_n}\right\| = 1.$$

In higher dimensions, initial positions of the point-particles can be visualized as vertices of a hypercube (orthotope), and their trajectories can be visualized through projection into a plane.

At the outset of each trial, the distance between particles is multiplied by a large constant to provide enough room for them to move during the course of the

analysis (the duration of the trial period). Technically, the distance between particles in their original configuration is the eigenvalue of the diagonal matrix describing the ensemble a time t = 0. We selected the value of 100.

Throughout the trial period, whenever a neuron $\vec{x_j}$ fired, it acquired a charge that was equivalent to a low-pass filtered version of its spike train. The charge q_j on any point-particle $\vec{x_j}$ at time *t* obeyed the equation

$$\frac{dq_j}{dt} = \frac{-q_j}{\tau},$$

where τ is the charge decay parameter. We selected a value of τ = 3 ms to reflect a short exponential decay period, although τ can be manipulated to control the influence of post-synaptic potential (PSP) on the simulation.

Particles moved in relation to the forces acting on them from all other charged particles. The force between any two point-particles $\vec{x_j}$ and $\vec{x_k}$ at time *t* was proportional to the product of their charges, acting on the unit vector $\hat{u}_{jk}$ on the line between them, described by the equation

$$\vec{f}_{jk}(t) = q_j q_k \hat{u}_{jk}.$$

The total force acting on the particle at time *t* was the sum of all pair-particle forces, or

$$\vec{f}_j^{total}(t) = q_j(t)\sum_{k\neq j}(q_k(t)\hat{u}_{jk}).$$

The algorithm treats the particles as if they were moving through a viscous medium, rather than a vacuum. This makes the velocity (rather than the acceleration) of each particle proportional to the total forces acting on it. The viscosity constant σ governs the quickness with which the particles move through the vector space. We set $\sigma = 0.5$, although the value may be manipulated for the purposes of the experiment. The velocity with which particle $\vec{x}_j$ moved at time *t* was given by

$$\vec{v}_j(t) = \frac{1}{\sigma}\vec{f}_j^{total}(t).$$

These conditions, in total, characterized the incremental distance Δs_j moved by particle $\vec{x}_j$ over the change in time Δt, which is the outcome of particle $\vec{x}_j$'s interaction with all other particles in the ensemble:

$$\Delta\vec{s}_j = \vec{v}_j(t)\Delta t \Leftrightarrow \frac{d\vec{s}_j}{dt} = \frac{1}{\sigma}\vec{f}_j^{total}(t).$$

We integrated over each Δt = 1ms interval and recorded particle movement throughout the trial period. Pair distances were recorded by registering the Euclidean distance between any two point-particles at each 1 ms interval, reflecting the coincidence structure of the ensemble activity.

Comprehensive significance envelope performance by millisecond-level class. The performance of each envelope is listed by its sensitivity to neuron-pair type. The correlation (*r)* values indicate the proportion of identical spikes between source-recipient pair spike trains.

		Envelope class					
	Correlation	Significant trials (%)			Significant ms/trial (ms)		
	r	*10 ms*	*15 ms*	*20 ms*	*10 ms*	*15 ms*	*20 ms*
PERFECT CORRELATION							
Neuron-pair type							
Visual-Visual	1	88.4	88.4	80.1	420	383	379
Visuomovement-	1	91.4	90.3	87.1	344	327	319
Visuomovement	1	61.0	64.0	58.7	249	214	206
Movement-Movement	1	88.6	88.6	88.3	339	340	328
Visual-Visuomovement	1	79.1	77.9	76.1	295	269	269
Visuomovement-Movement	1	91.0	92.4	92.4	331	295	288
Visual-Movement							
AVG		83.3	83.6	80.4	330	305	298
SCALED CORRELATION							
Neuron-pair type							
Visual-Visual	0.8	67.6	67.6	76.5	340	356	353
Visuomovement-	0.8	79.3	78.7	77.0	306	284	272
Visuomovement	0.8	36.5	40.4	40.4	223	184	194
Movement-Movement	0.6	62.7	63.3	61.3	240	227	215
Visual-Visuomovement	0.6	51.2	49.4	50.0	205	217	215
Visuomovement-Movement	0.4	58.0	50.0	52.0	135	117	102
Visual-Movement							
AVG		61.6	58.2	59.2	243	230	225
GRAND AVG		72.5	70.9	69.8	287	268	262

APPENDIX C

CUMULATIVE DENSITY PLOTS

In the following pages, the comprehensive results for cumulative density functions for synchrony and asynchrony are given (y-axis represents cumulative density for every plot, while align event is individually marked). On each page, the colored function corresponds to the overlapping receptive field condition for the neuron pair type. The colored but dashed function corresponds to the adjacent receptive field condition. Gray and black functions correspond to neutral and singleton receptive field conditions, respectively. Moreover, open circles represent peaks in the growth of synchrony, superimposed on the CDF for each receptive field condition. Finally, vertical gray lines indicate the time of average TDT for each condition.

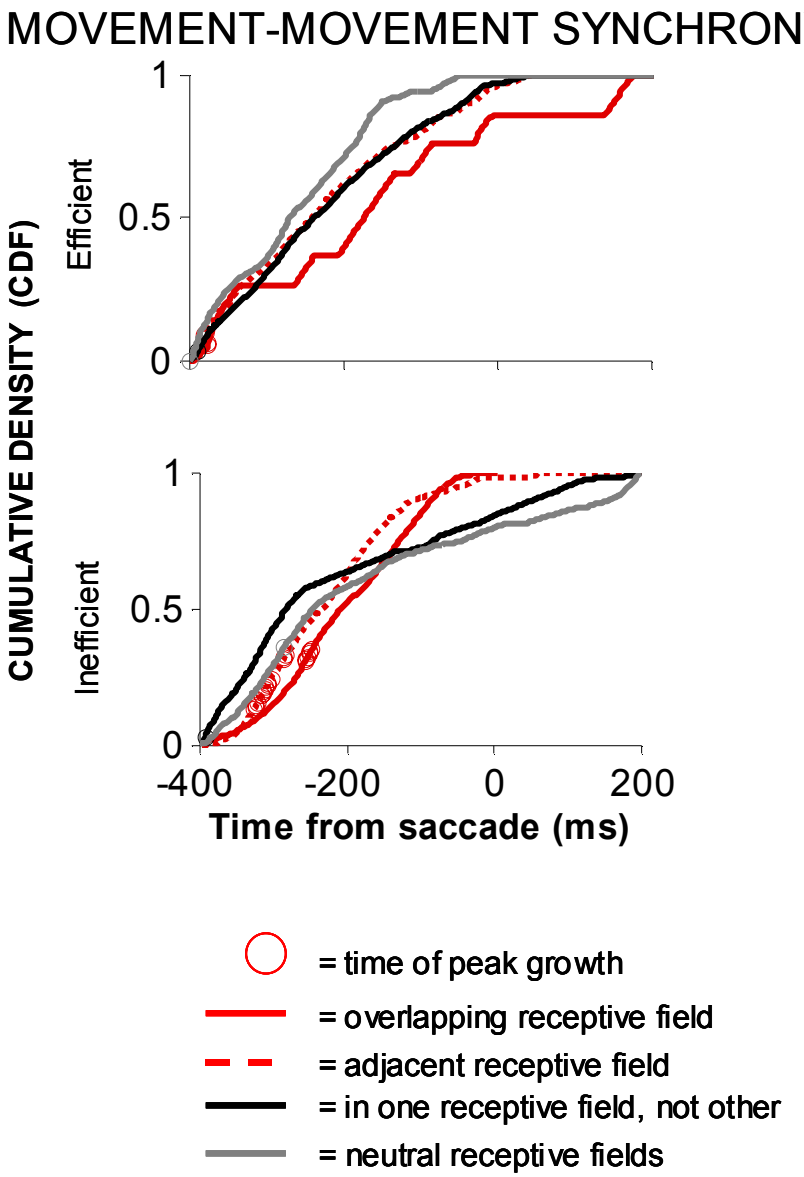
MOVEMENT-MOVEMENT SYNCHRONY
CUMULATIVE DENSITY (CDF)
Efficient
Inefficient
1
0.5
0
-400
-200
0
200
Time from saccade (ms)
= time of peak growth
= overlapping receptive field
= adjacent receptive field
= in one receptive field, not other
= neutral receptive fields

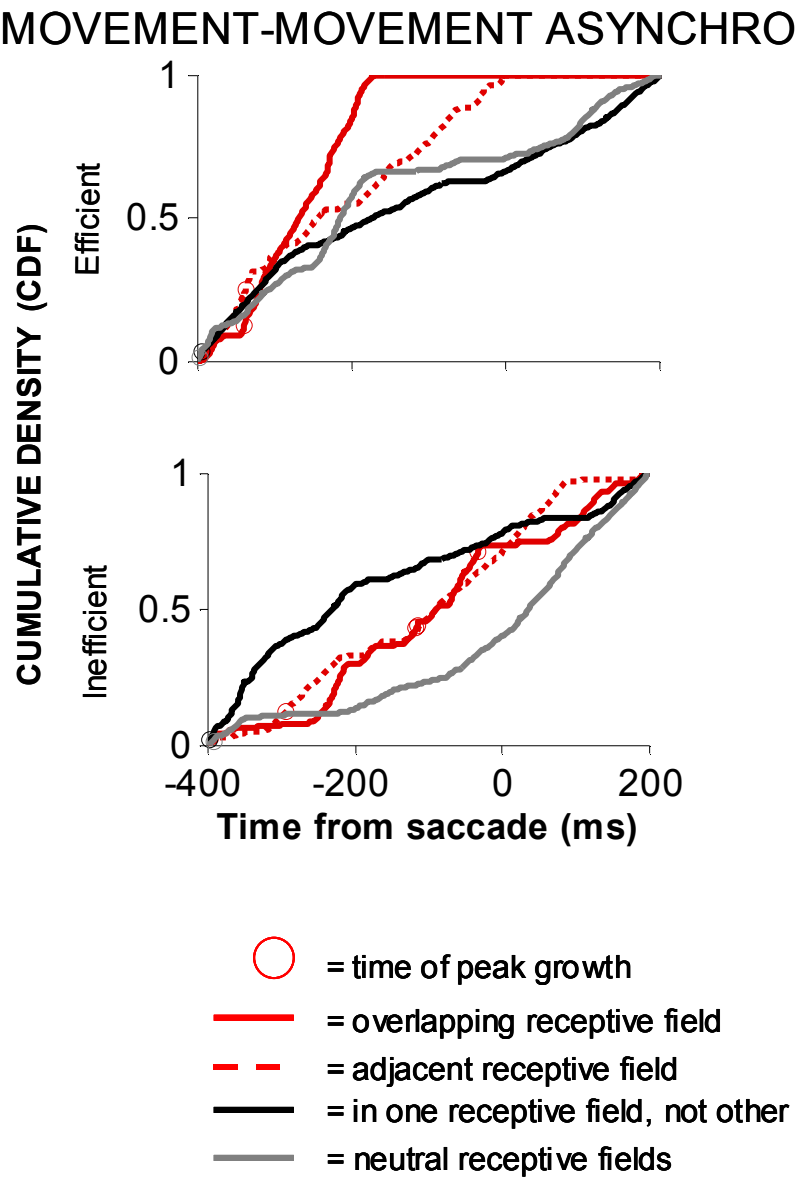
MOVEMENT-MOVEMENT ASYNCHRONY
CUMULATIVE DENSITY (CDF)
Efficient
Inefficient
1
0.5
0
-400
-200
0
200
Time from saccade (ms)
= time of peak growth
= overlapping receptive field
= adjacent receptive field
= in one receptive field, not other
= neutral receptive fields

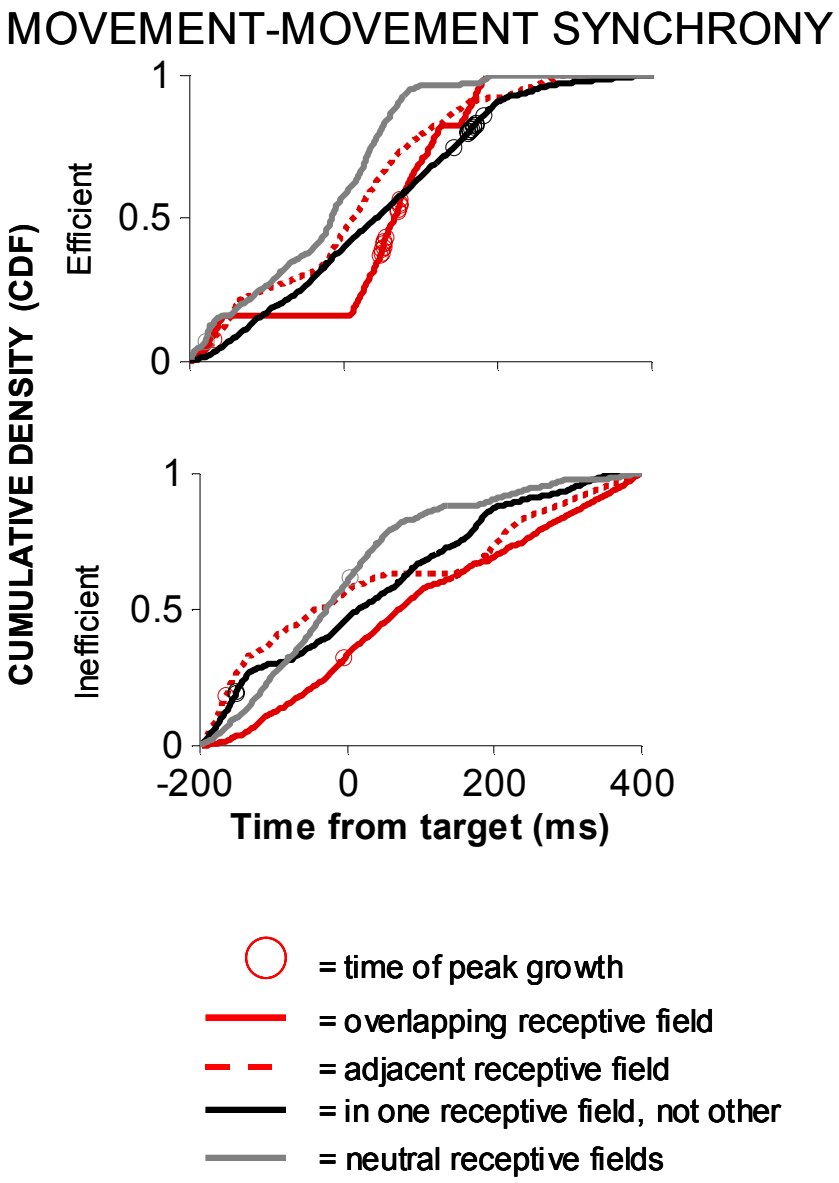
MOVEMENT-MOVEMENT SYNCHRONY
CUMULATIVE DENSITY (CDF)
Efficient
Inefficient
1
0.5
0
-200
0
200
400
Time from target (ms)
= time of peak growth
= overlapping receptive field
= adjacent receptive field
= in one receptive field, not other
= neutral receptive fields

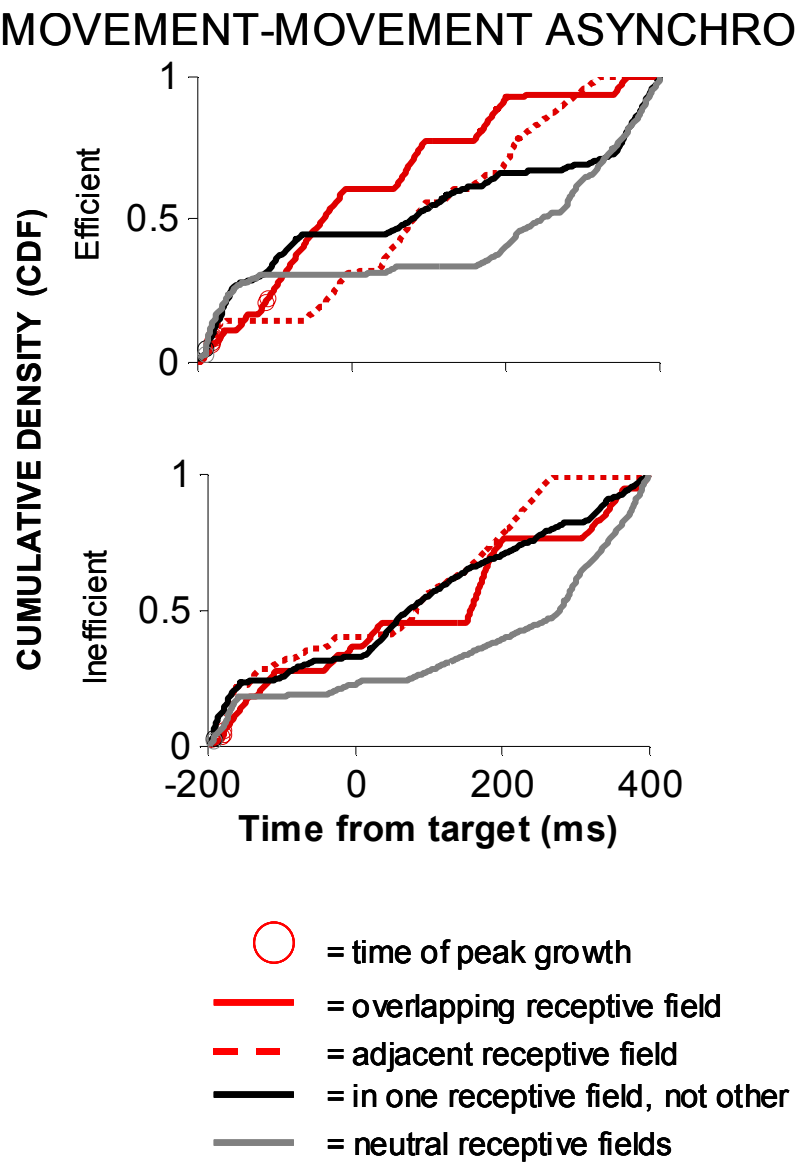
MOVEMENT-MOVEMENT ASYNCHRONY
CUMULATIVE DENSITY (CDF)
Efficient
Inefficient
1
0.5
0
-200
0
200
400
Time from target (ms)
= time of peak growth
= overlapping receptive field
= adjacent receptive field
= in one receptive field, not other
= neutral receptive fields

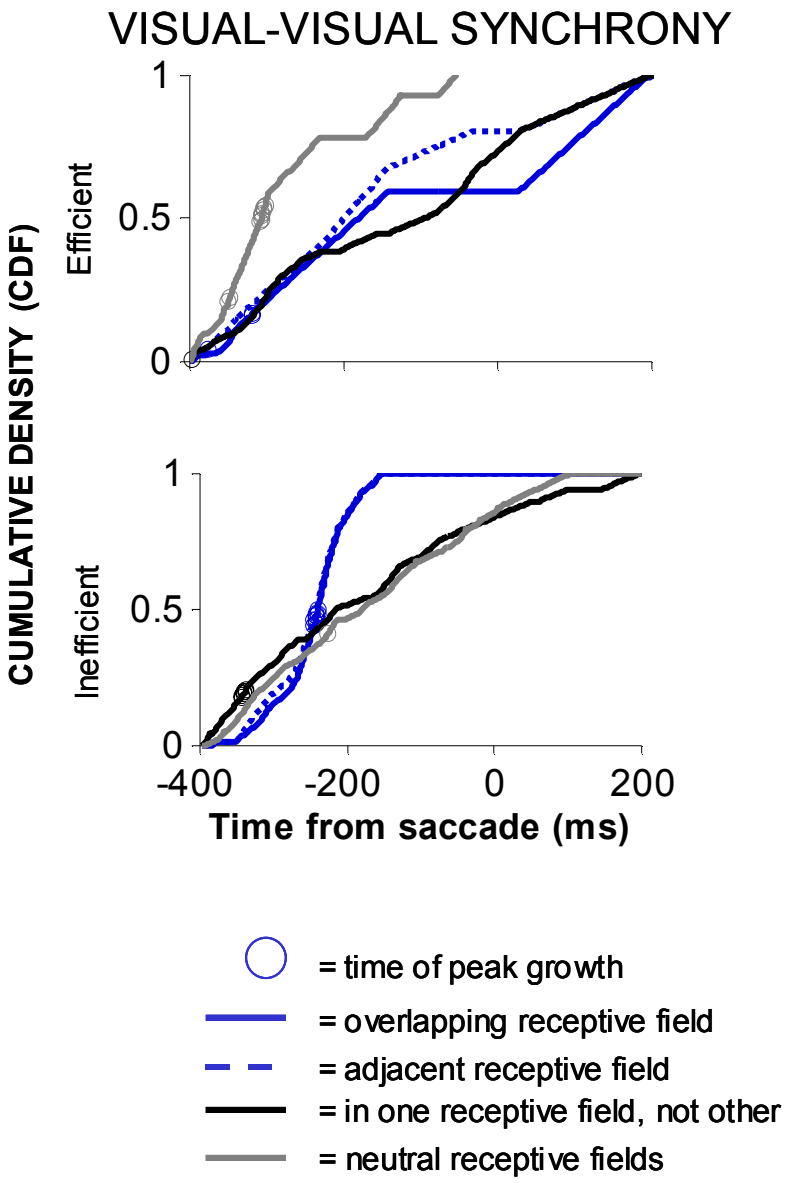
VISUAL-VISUAL SYNCHRONY
CUMULATIVE DENSITY (CDF)
Efficient
Inefficient
1
0.5
0
-400
-200
0
200
Time from saccade (ms)
= time of peak growth
= overlapping receptive field
= adjacent receptive field
= in one receptive field, not other
= neutral receptive fields

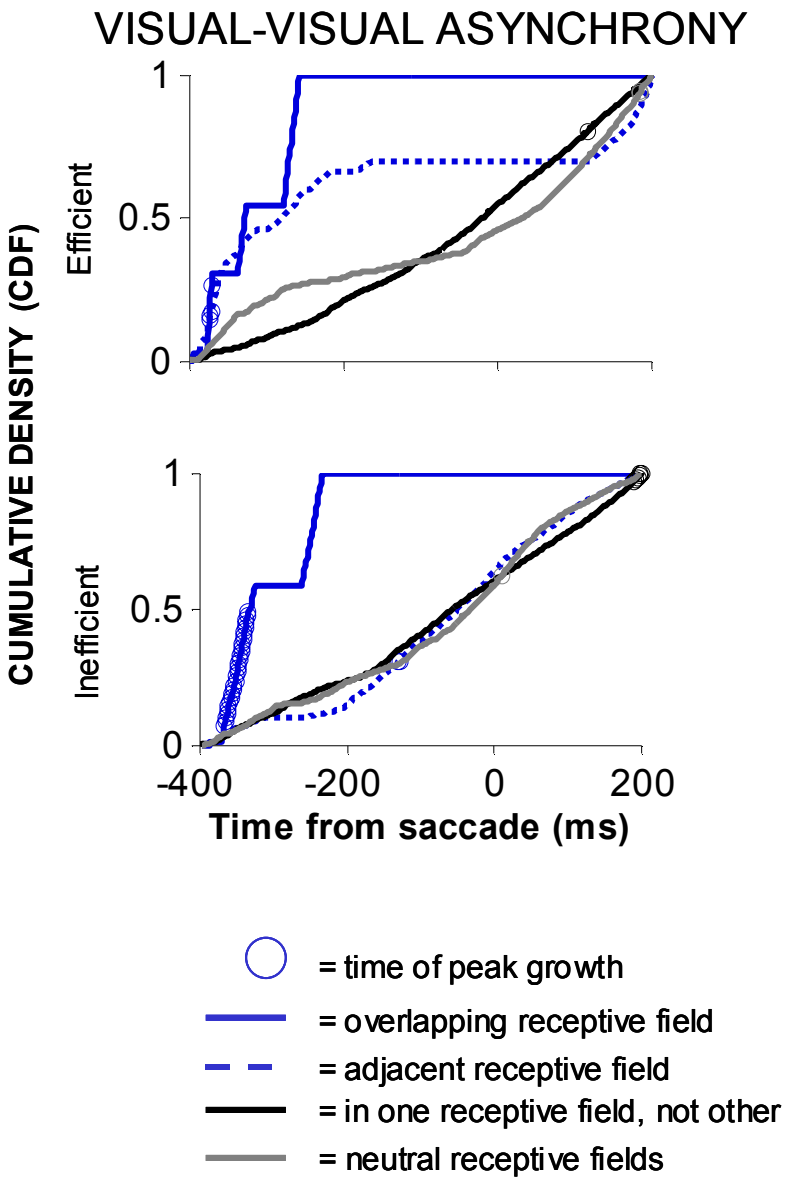
VISUAL-VISUAL ASYNCHRONY
CUMULATIVE DENSITY (CDF)
Efficient
Inefficient
1
0.5
0
-400
-200
0
200
Time from saccade (ms)
= time of peak growth
= overlapping receptive field
= adjacent receptive field
= in one receptive field, not other
= neutral receptive fields

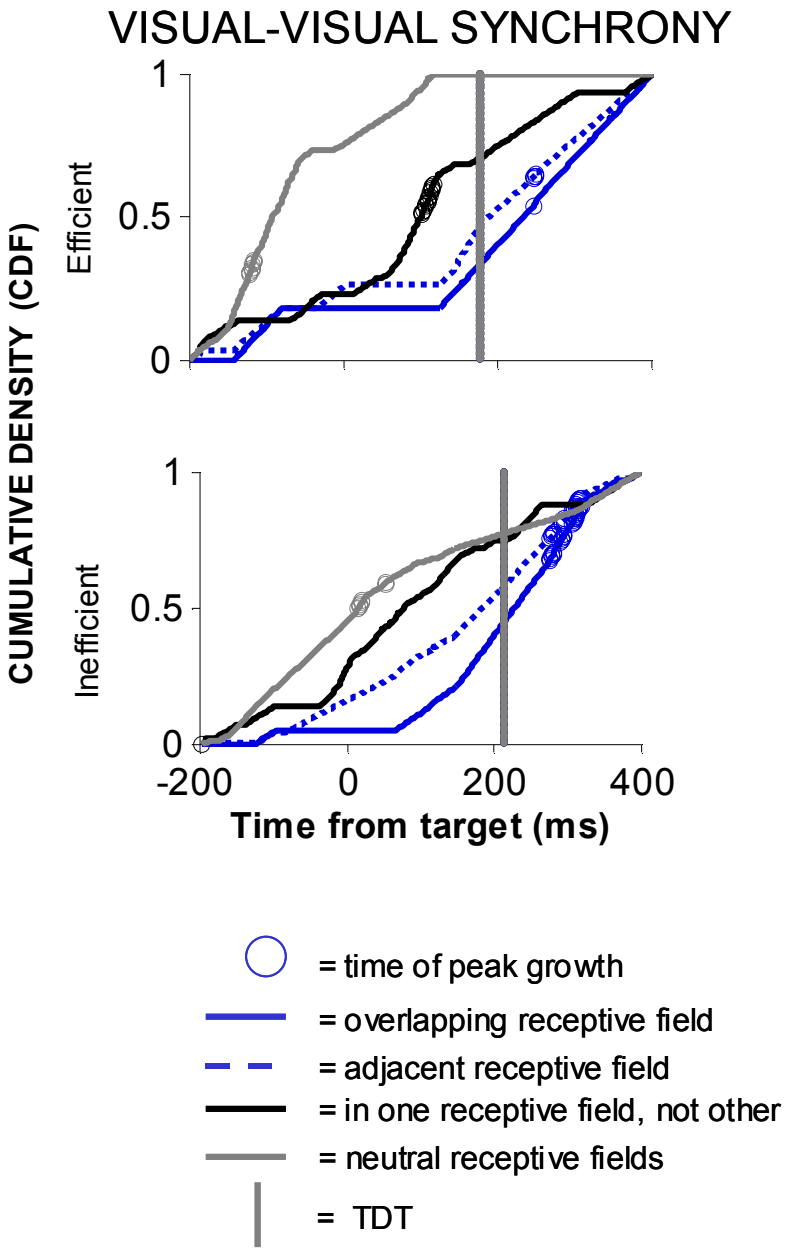
VISUAL-VISUAL SYNCHRONY
CUMULATIVE DENSITY (CDF)
Efficient
Inefficient
1
0.5
0
-200
0
200
400
Time from target (ms)
= time of peak growth
= overlapping receptive field
= adjacent receptive field
= in one receptive field, not other
= neutral receptive fields
= TDT

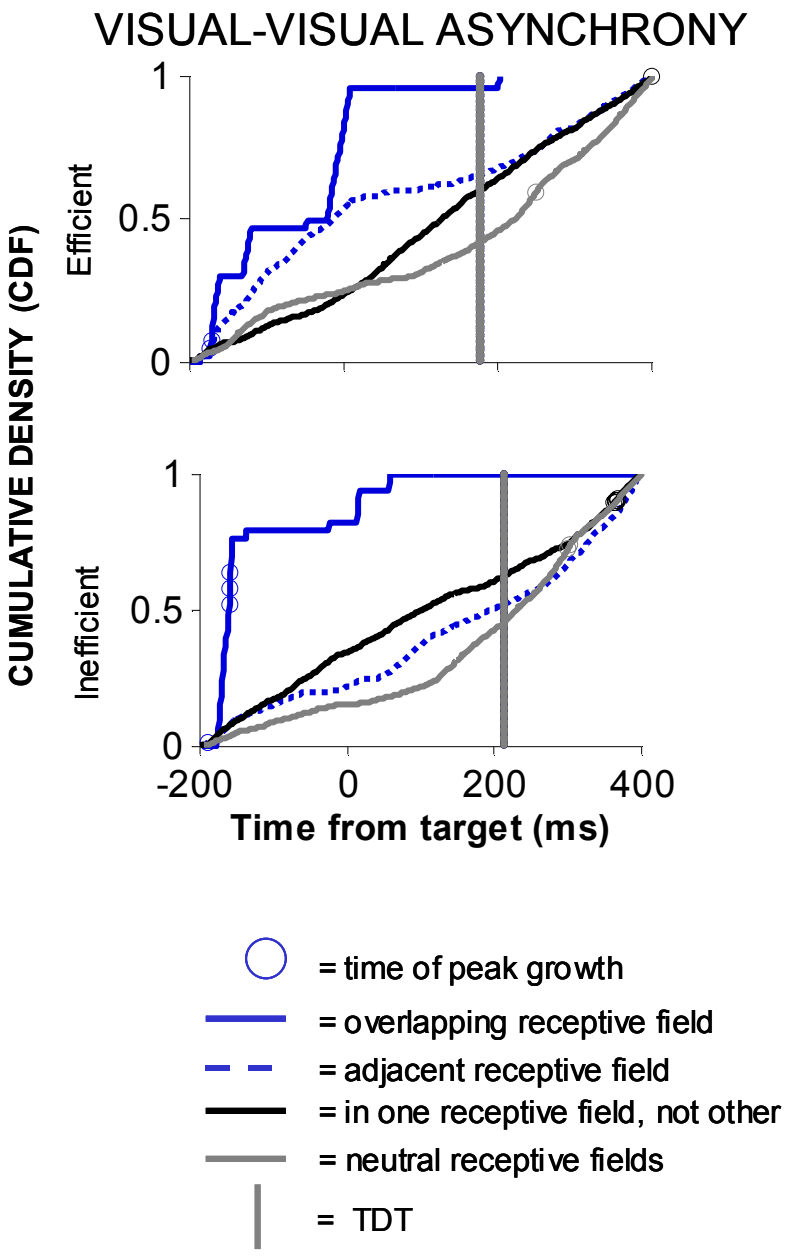
VISUAL-VISUAL ASYNCHRONY
CUMULATIVE DENSITY (CDF)
Efficient
Inefficient
1
0.5
0
-200
0
200
400
Time from target (ms)
= time of peak growth
= overlapping receptive field
= adjacent receptive field
= in one receptive field, not other
= neutral receptive fields
= TDT

VISUOMOVEMENT-VISUOMOVEMENT SYNCHRONY

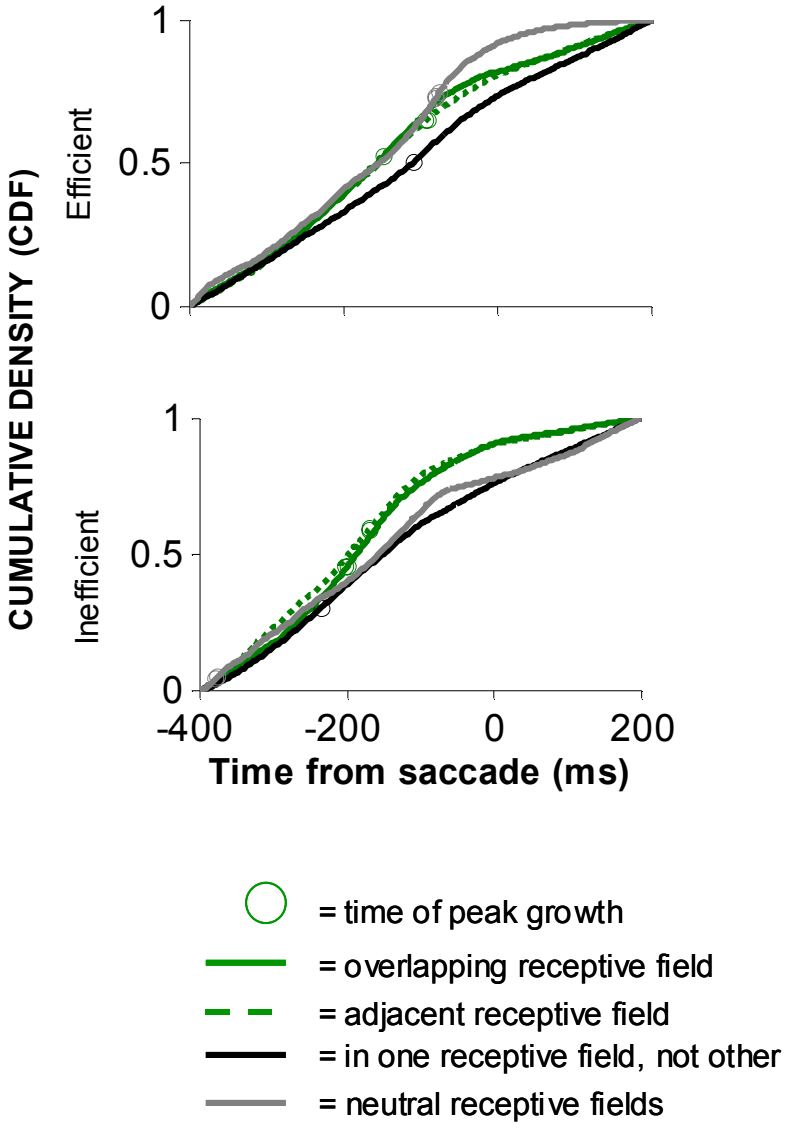

VISUOMOVEMENT-VISUOMOVEMENT ASYNCHRONY

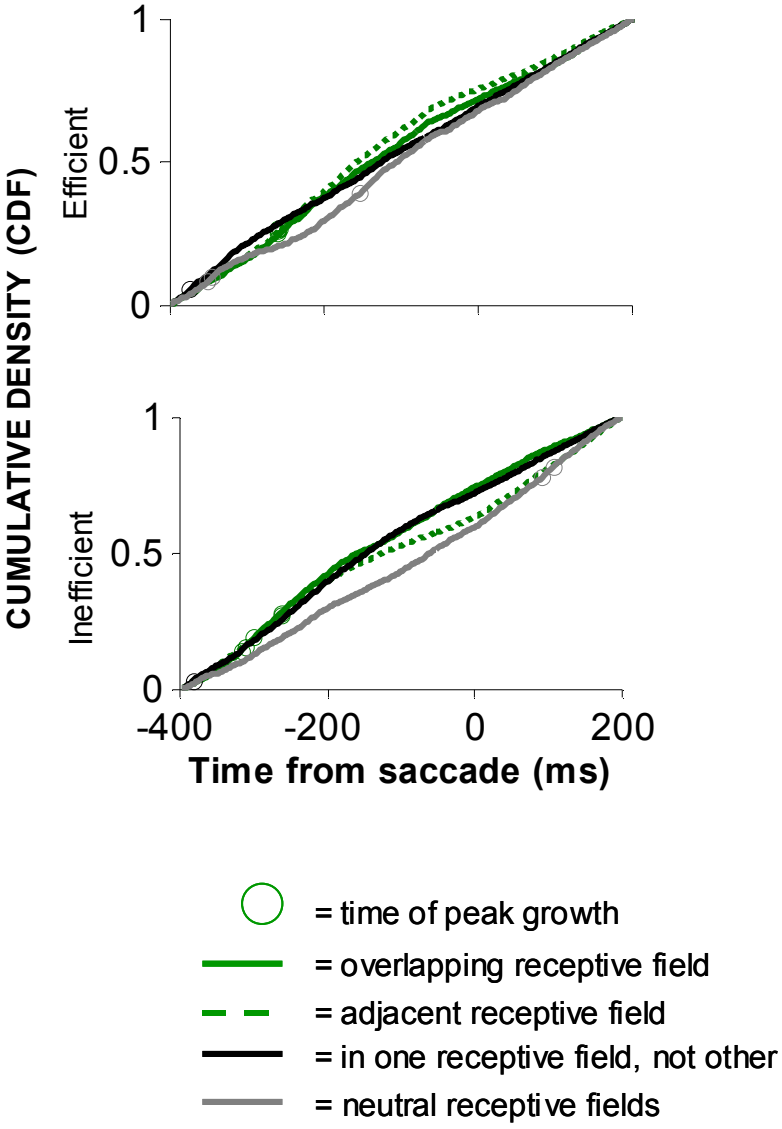

VISUOMOVEMENT-VISUOMOVEMENT SYNCHRONY

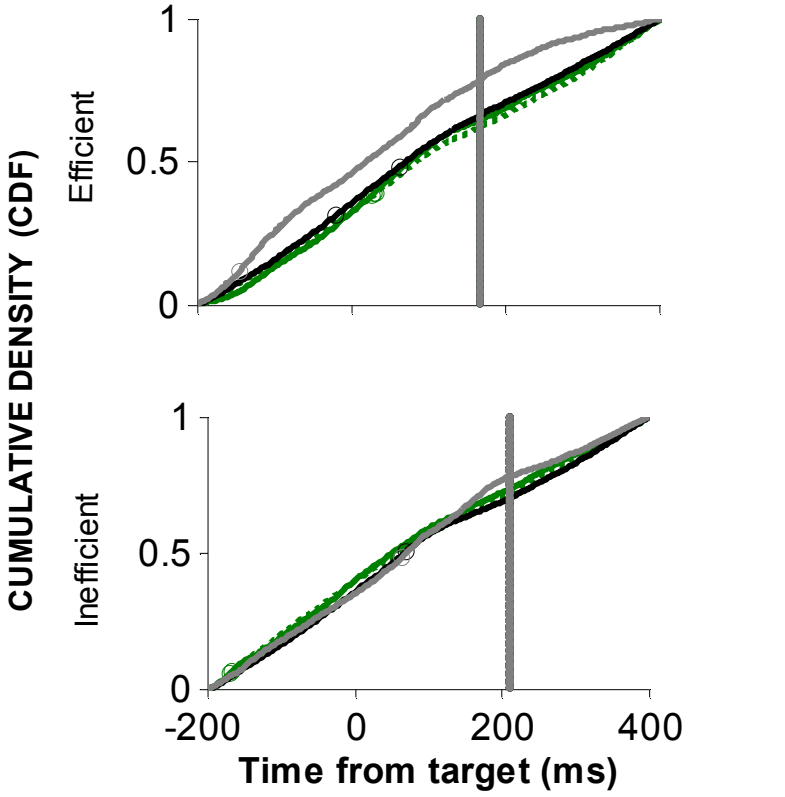

= time of peak growth
= overlapping receptive field
= adjacent receptive field
= in one receptive field, not other
= neutral receptive fields
= TDT

VISUOMOVEMENT-VISUOMOVEMENT ASYNCHRONY

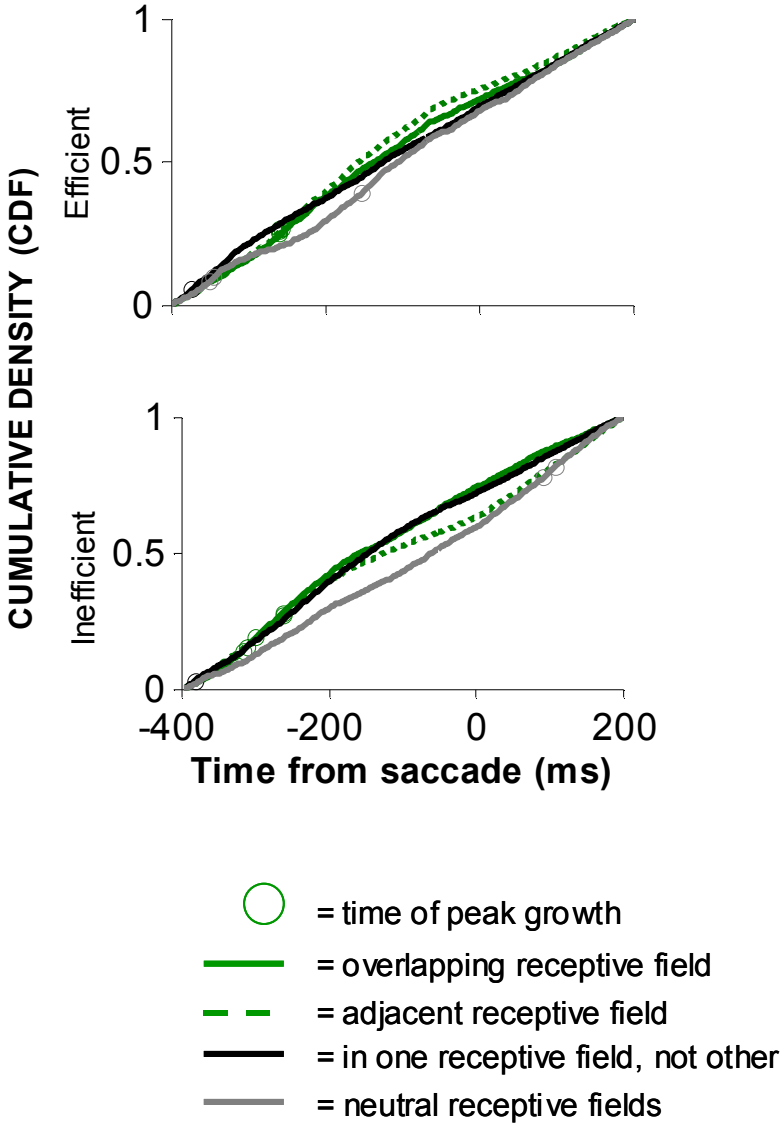

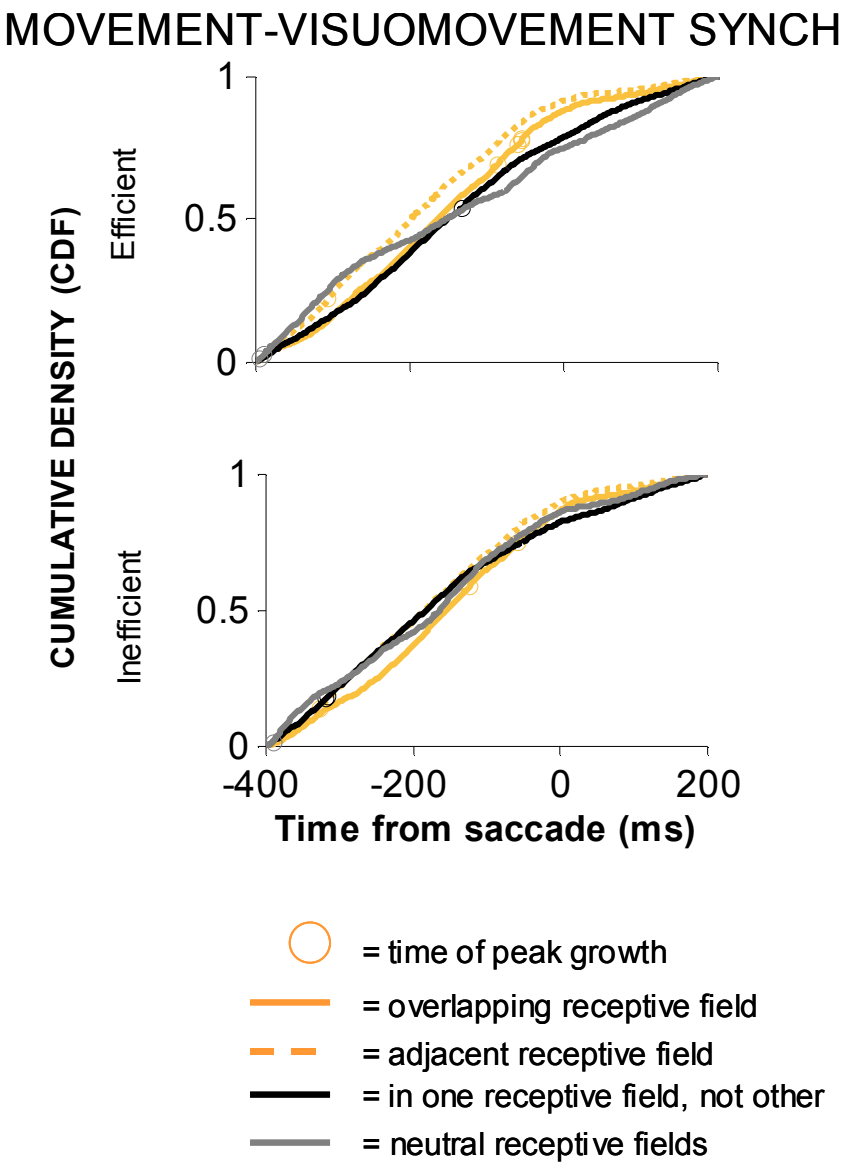
MOVEMENT-VISUOMOVEMENT SYNCHRONY
CUMULATIVE DENSITY (CDF)
Efficient
Inefficient
1
0.5
0
-400
-200
0
200
Time from saccade (ms)
= time of peak growth
= overlapping receptive field
= adjacent receptive field
= in one receptive field, not other
= neutral receptive fields

MOVEMENT-VISUOMOVEMENT ASYNCHRONY

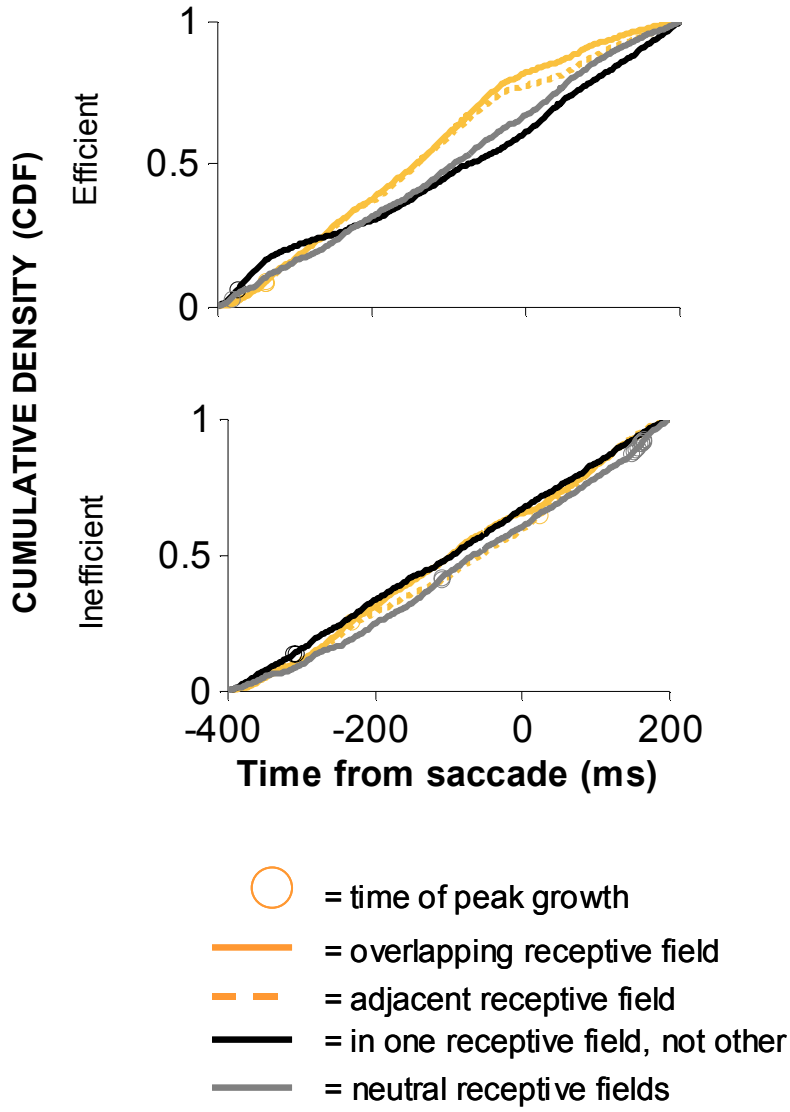

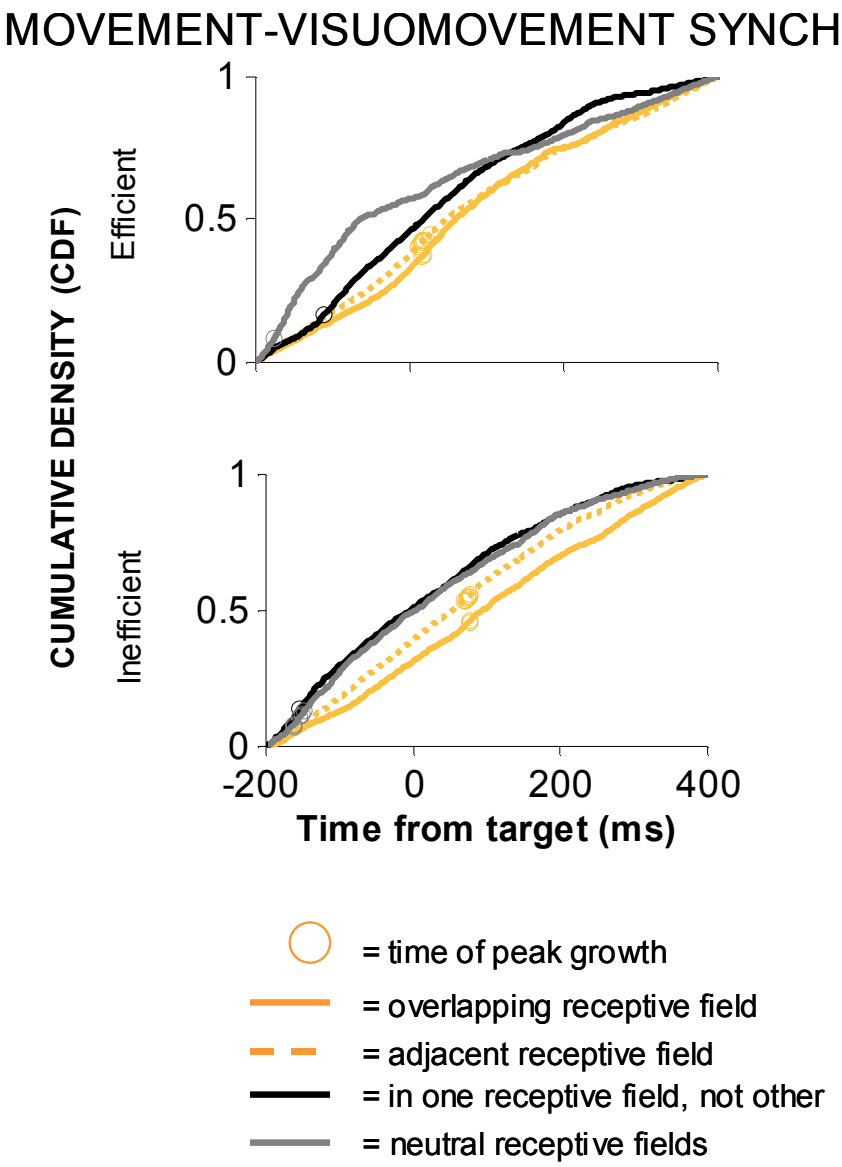
MOVEMENT-VISUOMOVEMENT SYNCHRONY
CUMULATIVE DENSITY (CDF)
Efficient
Inefficient
1
0.5
0
-200
0
200
400
Time from target (ms)
= time of peak growth
= overlapping receptive field
= adjacent receptive field
= in one receptive field, not other
= neutral receptive fields

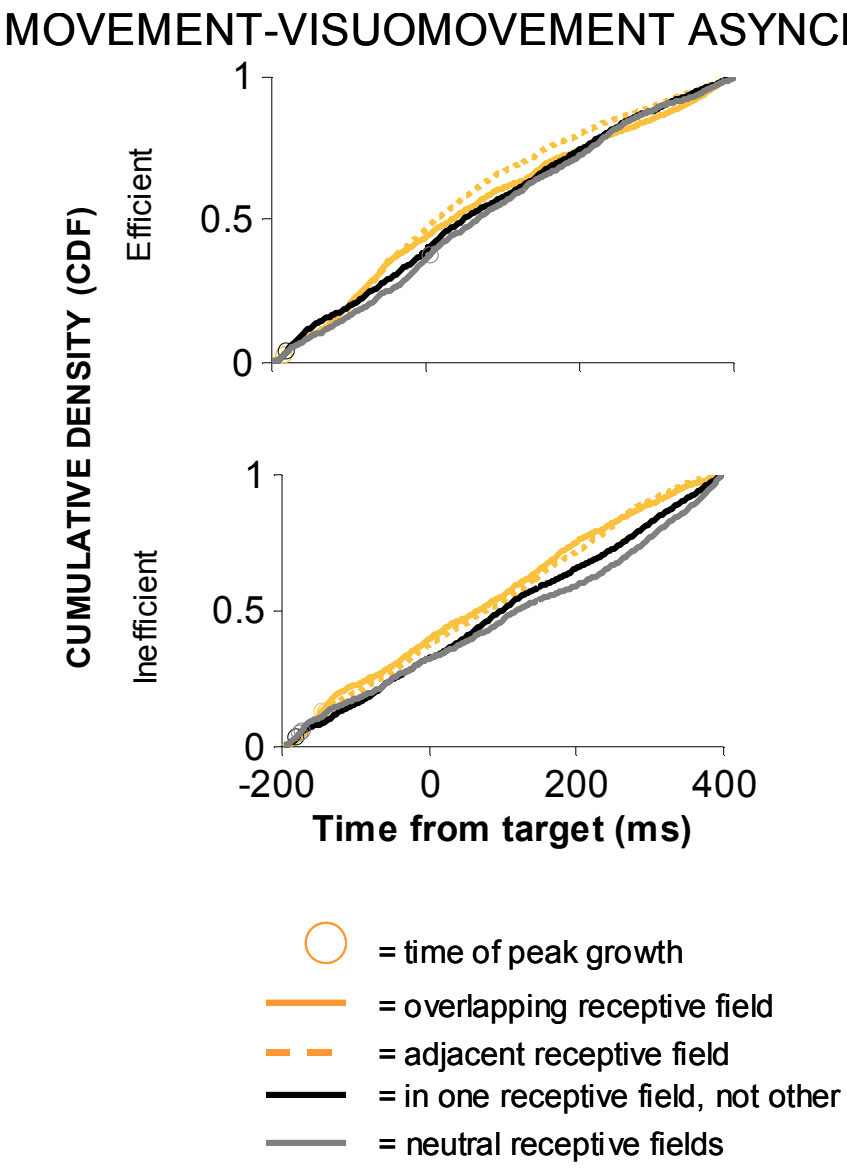
MOVEMENT-VISUOMOVEMENT ASYNCHRONY
CUMULATIVE DENSITY (CDF)
Efficient
Inefficient
1
0.5
0
-200
0
200
400
Time from target (ms)
= time of peak growth
= overlapping receptive field
= adjacent receptive field
= in one receptive field, not other
= neutral receptive fields

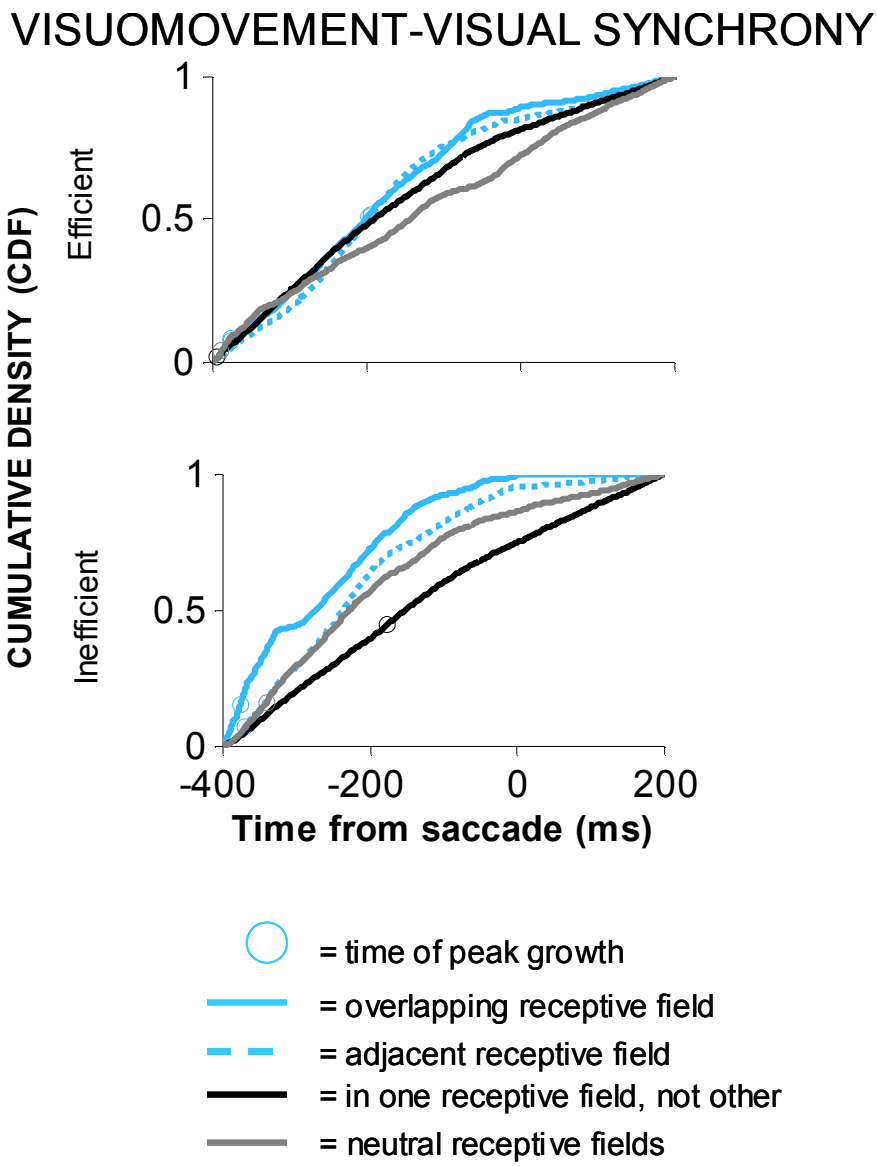
VISUOMOVEMENT-VISUAL SYNCHRONY
CUMULATIVE DENSITY (CDF)
Efficient
Inefficient
1
0.5
0
-400
-200
0
200
Time from saccade (ms)
= time of peak growth
= overlapping receptive field
= adjacent receptive field
= in one receptive field, not other
= neutral receptive fields

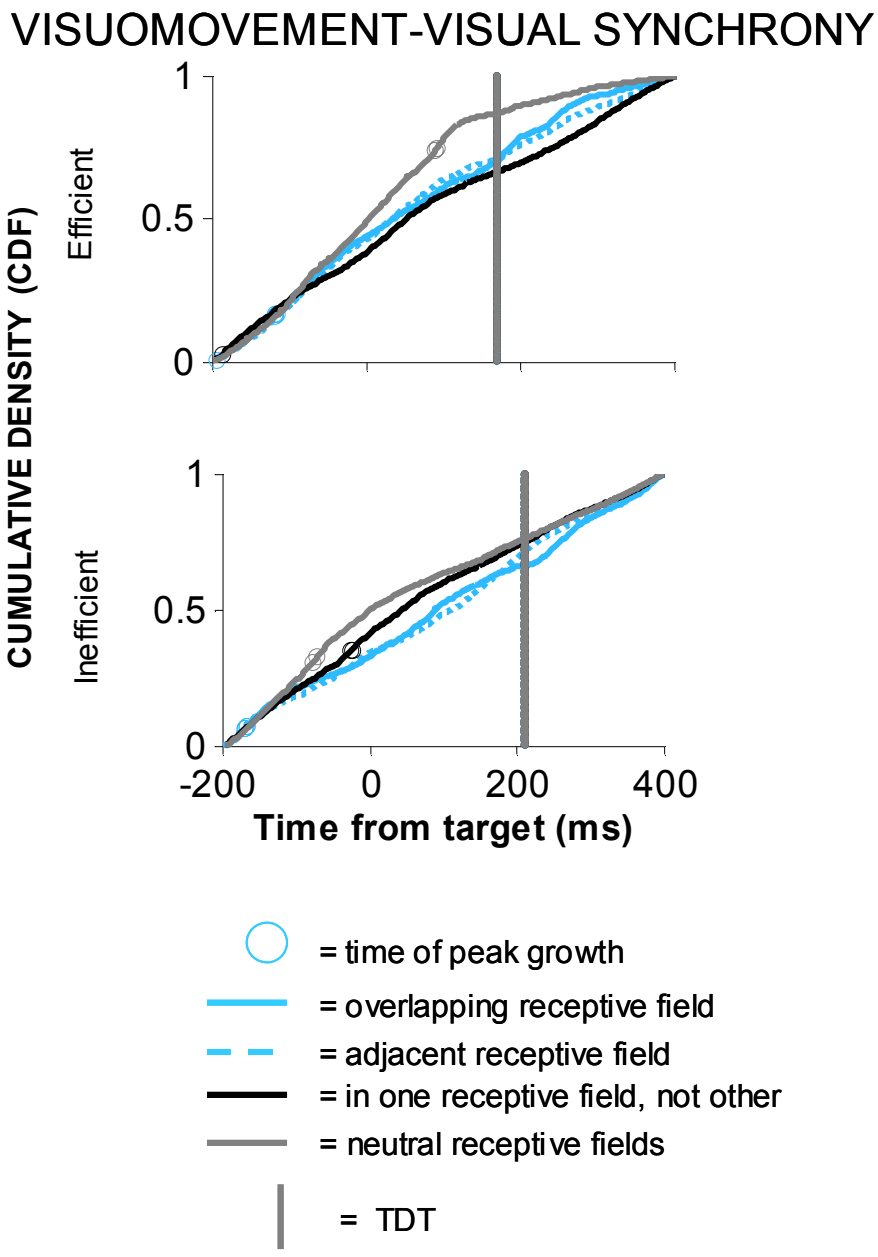
VISUOMOVEMENT-VISUAL SYNCHRONY
CUMULATIVE DENSITY (CDF)
Efficient
Inefficient
1
0.5
0
-200
0
200
400
Time from target (ms)
= time of peak growth
= overlapping receptive field
= adjacent receptive field
= in one receptive field, not other
= neutral receptive fields
= TDT

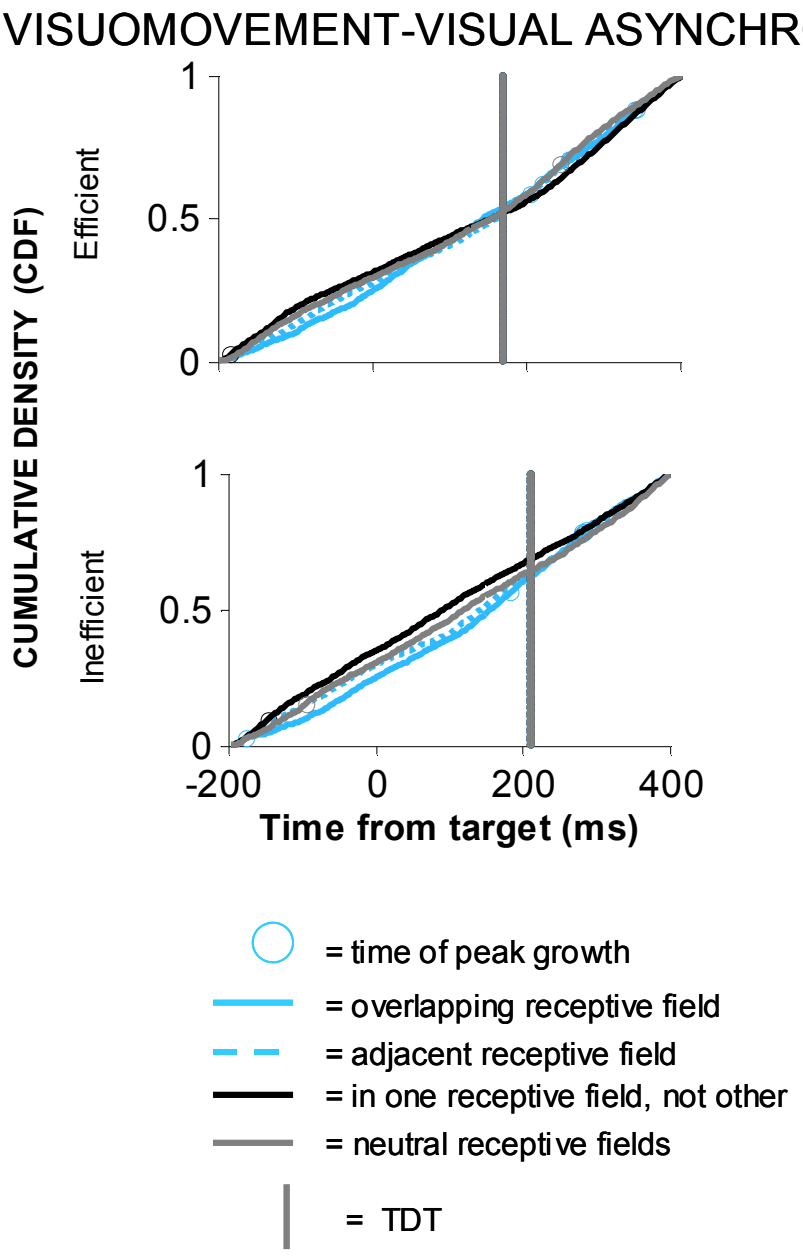
VISUOMOVEMENT-VISUAL ASYNCHRONY
CUMULATIVE DENSITY (CDF)
Efficient
Inefficient
1
0.5
0
-200
0
200
400
Time from target (ms)
= time of peak growth
= overlapping receptive field
= adjacent receptive field
= in one receptive field, not other
= neutral receptive fields
= TDT

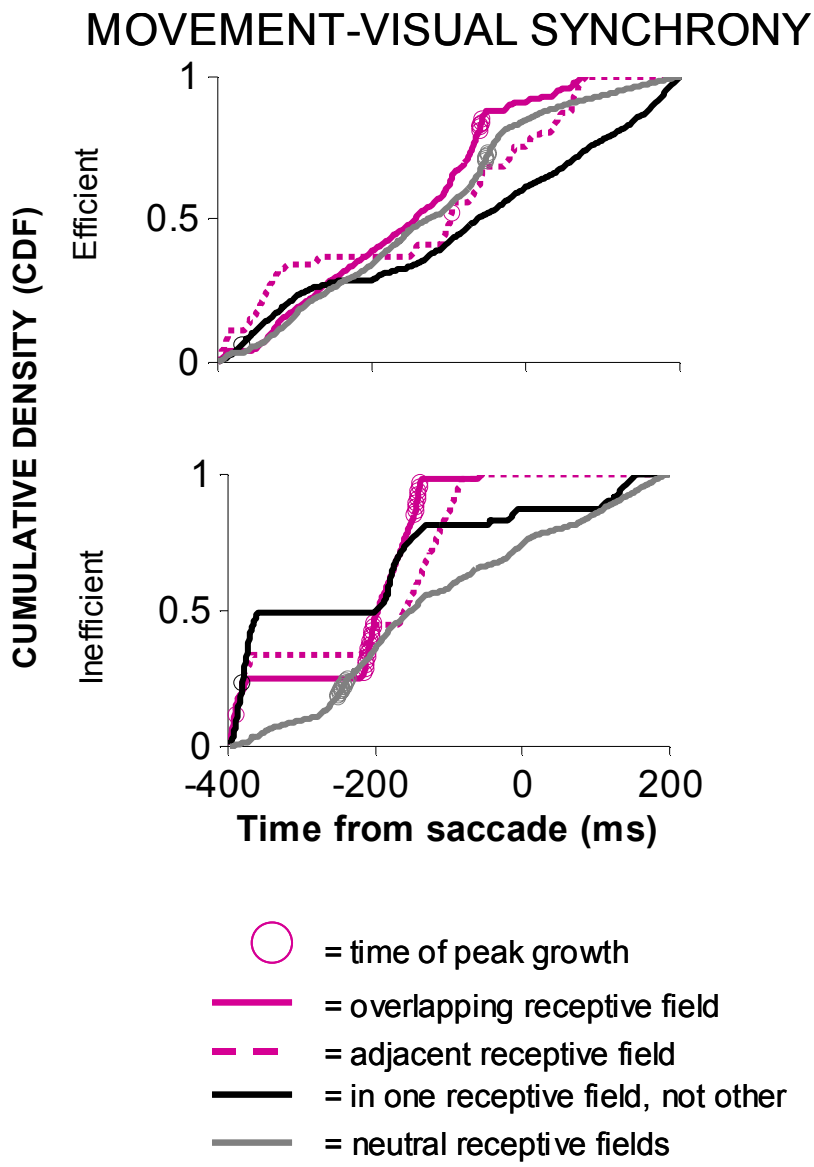
MOVEMENT-VISUAL SYNCHRONY
CUMULATIVE DENSITY (CDF)
Efficient
Inefficient
1
0.5
0
1
0.5
0
-400
-200
0
200
Time from saccade (ms)
= time of peak growth
= overlapping receptive field
= adjacent receptive field
= in one receptive field, not other
= neutral receptive fields

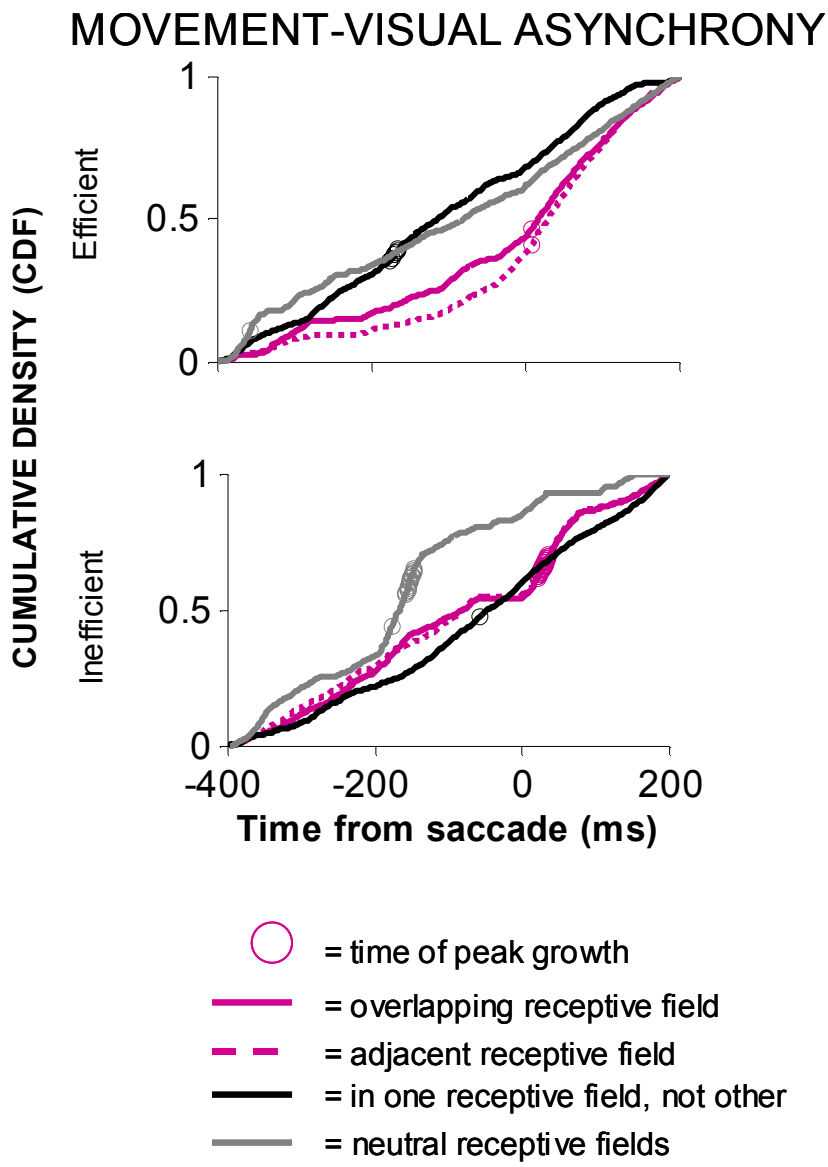
MOVEMENT-VISUAL ASYNCHRONY
CUMULATIVE DENSITY (CDF)
Efficient
Inefficient
1
0.5
0
-400
-200
0
200
Time from saccade (ms)
= time of peak growth
= overlapping receptive field
= adjacent receptive field
= in one receptive field, not other
= neutral receptive fields

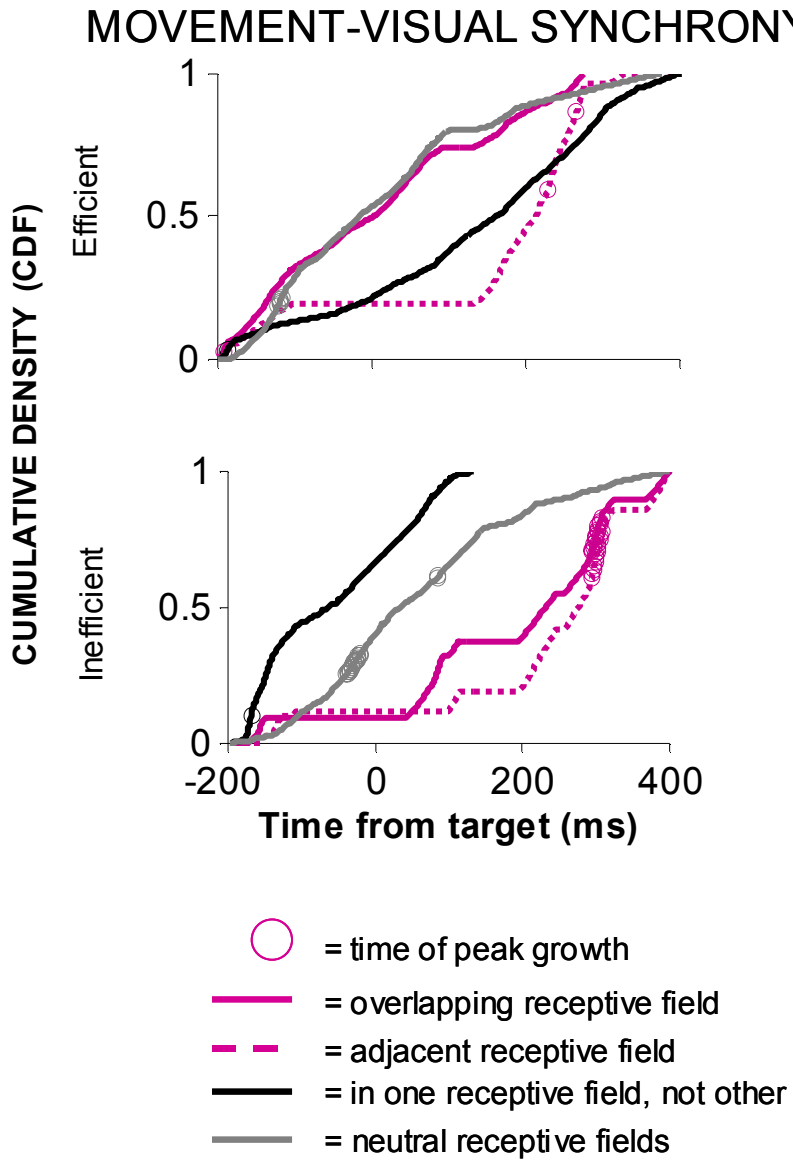
MOVEMENT-VISUAL SYNCHRONY
CUMULATIVE DENSITY (CDF)
Efficient
Inefficient
1
0.5
0
-200
0
200
400
Time from target (ms)
= time of peak growth
= overlapping receptive field
= adjacent receptive field
= in one receptive field, not other
= neutral receptive fields

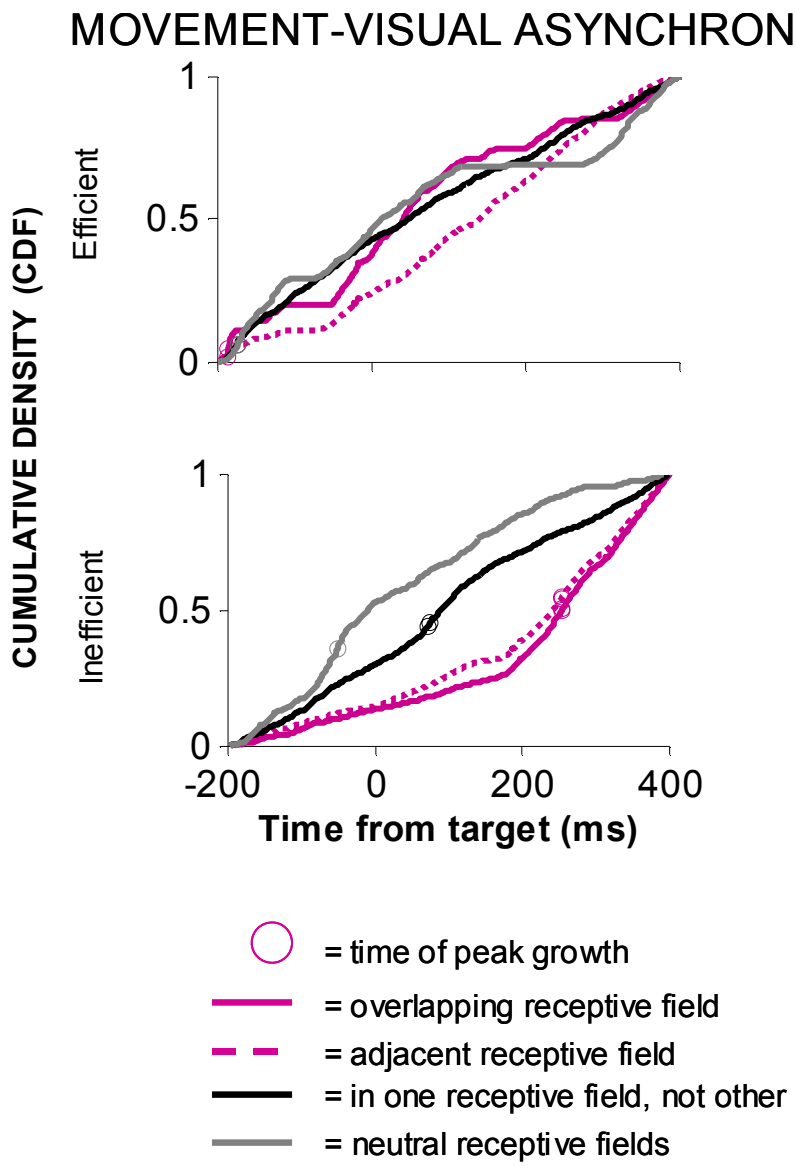
MOVEMENT-VISUAL ASYNCHRONY
CUMULATIVE DENSITY (CDF)
Efficient
Inefficient
1
0.5
0
-200
0
200
400
Time from target (ms)
= time of peak growth
= overlapping receptive field
= adjacent receptive field
= in one receptive field, not other
= neutral receptive fields

	THEORY OR OBSERVATION	RELEVANT EVENT OR PROCESS	CELL-CLASS INTERACTION	RECEPTIVE FIELD ORGANIZATION IN RELATION TO TARGET	SEARCH EFFICIENCY	*Prediction* SYNCH.
i.	Stereotyped latency for onset of visual activity in FEF (Thompson et al. 1996; Schmolesky et al. 1998; Pouget et al. 2005)	35-70 ms after target onset	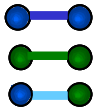	✓OVERLAPPING ?ADJACENT	----- No initial target selectivity (Schall & Hanes 1993; Schall et al. 1995 b)	↑
ii.	Synchrony in topographically organized sub-networks/modules (Yoshimura et al. 2005)					
i.	Synchrony as mechanism for selective attention (Niebur 2002)	Target selection, at or around previously established TDT times		✓OVERLAPPING ✓NEUTRAL ✓IN ONE ONLY ØADJACENT (surround supp.)	 With peak synch. in efficient search closer to target onset	↑
ii.	Synchrony as mechanism for parallel distribution of selective visual attention in search (Bichot et al. 2005)					
i.	Surround suppression increases with target proximity (Schall et al. 1995b), but not search efficiency (Schall et al. 2004)	Target discrimination process		✓ADJACENT ØOVERLAPPING ØNEUTRAL ØIN ONE ONLY	----	↓
i.	Continuous processing during sensorimotor transformation (Bichot et al. 2001b), movement neuron activity enhanced in conjunction search when similar distractor in RF	Target discrimination and saccade preparation		✓NEUTRAL ✓IN ONE ONLY ✓ADJACENT (distractor in at least one RF in each condition)	 No singleton distractor to bias bottom-up distractor salience in efficient search	↑
i.	Continuous processing during sensorimotor transformation (Bichot et al. 2001b)	Saccade planning and initiation		✓OVERLAPPING	 With peak synch. in inefficient search closer to saccade initiation	↑
ii.	Enhanced activity for target appearing in response field of movement neuron prior to saccade					
iii.	Topographic map in FEF where amplitude and direction of saccades organized retinotopically (Bruce et al. 1985)					

REFERENCES

Abeles, M. 1982. Role of the cortical neuron: integrator or coincidence detector? Isr J Med Sci 18 (1):83-92.

Aertsen, A. M., G. L. Gerstein, M. K. Habib, and G. Palm. 1989. Dynamics of neuronal firing correlation: modulation of "effective connectivity". J Neurophysiol 61 (5):900-17.

Aertsen, A., and M. Arndt. 1993. Response synchronization in the visual cortex. Curr Opin Neurobiol 3 (4):586-94.

Aertsen, A., M. Diesmann, and M. O. Gewaltig. 1996. Propagation of synchronous spiking activity in feedforward neural networks. J Physiol Paris 90 (3-4):243-7.

Alonso, J. M., W. M. Usrey, and R. C. Reid. 1996. Precisely correlated firing in cells of the lateral geniculate nucleus. Nature 383 (6603):815-9.

Arata, A., Y. M. Hernandez, B. G. Lindsey, K. F. Morris, and R. Shannon. 2000. Transient configurations of baroresponsive respiratory-related brainstem neuronal assemblies in the cat. J Physiol 525 Pt 2:509-30.

Azouz, R., and C. M. Gray. 1999. Cellular mechanisms contributing to response variability of cortical neurons in vivo. J Neurosci 19 (6):2209-23.

Azouz, R., and C. M. Gray. 1999. 2000. Dynamic spike threshold reveals a mechanism for synaptic coincidence detection in cortical neurons in vivo. Proc Natl Acad Sci U S A 97 (14):8110-5.

Azouz, R., and C. M. Gray. 1999. 2003. Adaptive coincidence detection and dynamic gain control in visual cortical neurons in vivo. Neuron 37 (3):513-23.

Bichot, N. P., and J. D. Schall. 1999. Effects of similarity and history on neural mechanisms of visual selection. Nat Neurosci 2 (6):549-54.

Bichot, N. P., K. G. Thompson, S. Chenchal Rao, and J. D. Schall. 2001. Reliability of macaque frontal eye field neurons signaling saccade targets during visual search. J Neurosci 21 (2):713-25.

Bichot, N. P., S. Chenchal Rao, and J. D. Schall. 2001. Continuous processing in macaque frontal cortex during visual search. Neuropsychologia 39 (9):972-82.

Bichot, N. P., A. F. Rossi, and R. Desimone. 2005. Parallel and serial neural mechanisms for visual search in macaque area V4. Science 308 (5721):529-34.

Binzegger, T., R. J. Douglas, and K. A. Martin. 2004. A quantitative map of the circuit of cat primary visual cortex. J Neurosci 24 (39):8441-53.

Britten, K. H., M. N. Shadlen, W. T. Newsome, and J. A. Movshon. 1992. The analysis of visual motion: a comparison of neuronal and psychophysical performance. J Neurosci 12 (12):4745-65.

Brown, E. N., R. E. Kass, and P. P. Mitra. 2004. Multiple neural spike train data analysis: state-of-the-art and future challenges. Nat Neurosci 7 (5):456-61.

Bruce, C. J., M. E. Goldberg, M. C. Bushnell, and G. B. Stanton. 1985. Primate frontal eye fields. II. Physiological and anatomical correlates of electrically evoked eye movements. J Neurophysiol 54 (3):714-34.

Burton, H., and R. J. Sinclair. 2000. Tactile-spatial and cross-modal attention effects in the primary somatosensory cortical areas 3b and 1-2 of rhesus monkeys. Somatosens Mot Res 17 (3):213-28.

Coss, R. G., and D. H. Perkel. 1985. The function of dendritic spines: a review of theoretical issues. Behav Neural Biol 44 (2):151-85.

Crist, C. F., D. S. Yamasaki, H. Komatsu, and R. H. Wurtz. 1988. A grid system and a microsyringe for single cell recording. J Neurosci Methods 26 (2):117-22.

Dan, Y., J. M. Alonso, W. M. Usrey, and R. C. Reid. 1998. Coding of visual information by precisely correlated spikes in the lateral geniculate nucleus. Nat Neurosci 1 (6):501-7.

Desimone, R., and J. Duncan. 1995. Neural mechanisms of selective visual attention. Annu Rev Neurosci 18:193-222.

Duncan, J., and G. W. Humphreys. 1989. Visual search and stimulus similarity. Psychol Rev 96 (3):433-58.

Engel, A. K., P. Konig, and W. Singer. 1991. Direct physiological evidence for scene segmentation by temporal coding. Proc Natl Acad Sci U S A 88 (20):9136-40.

Engel, A. K., P. Fries, and W. Singer. 2001. Dynamic predictions: oscillations and synchrony in top-down processing. Nat Rev Neurosci 2 (10):704-16.

Fries, P., J. H. Reynolds, A. E. Rorie, and R. Desimone. 2001. Modulation of oscillatory neuronal synchronization by selective visual attention. Science 291 (5508):1560-3.

Georgopoulos, A. P., R. E. Kettner, and A. B. Schwartz. 1988. Primate motor cortex and free arm movements to visual targets in three-dimensional space. II. Coding of the direction of movement by a neuronal population. J Neurosci 8 (8):2928-37.

Gerstein, G. L., and D. H. Perkel. 1969. Simultaneously recorded trains of action potentials: analysis and functional interpretation. Science 164 (881):828-30.

Gerstein, G. L., and D. H. Perkel. 1972. Mutual temporal relationships among neuronal spike trains. Statistical techniques for display and analysis. Biophys J 12 (5):453-73.

Gerstein, G. L., D. H. Perkel, and J. E. Dayhoff. 1985. Cooperative firing activity in simultaneously recorded populations of neurons: detection and measurement. J Neurosci 5 (4):881-9.

Grammont, F., and A. Riehle. 2003. Spike synchronization and firing rate in a population of motor cortical neurons in relation to movement direction and reaction time. Biol Cybern 88 (5):360-73.

Gray, C. M., A. K. Engel, P. Konig, and W. Singer. 1992. Synchronization of oscillatory neuronal responses in cat striate cortex: temporal properties. Vis Neurosci 8 (4):337-47.

Hanes, D. P., and J. D. Schall. 1996. Neural control of voluntary movement initiation. Science 274 (5286):427-30.

Hellwig, B., A. Schuz, and A. Aertsen. 1994. Synapses on axon collaterals of pyramidal cells are spaced at random intervals: a Golgi study in the mouse cerebral cortex. Biol Cybern 71 (1):1-12.

Hsiao, S. S., D. M. O'Shaughnessy, and K. O. Johnson. 1993. Effects of selective attention on spatial form processing in monkey primary and secondary somatosensory cortex. J Neurophysiol 70 (1):444-7.

Kastner, S., and L. G. Ungerleider. 2000. Mechanisms of visual attention in the human cortex. Annu Rev Neurosci 23:315-41.

Koch, C., M. Rapp, and I. Segev. 1996. A brief history of time (constants). Cereb Cortex 6 (2):93-101.

Konig, P., A. K. Engel, and W. Singer. 1996. Integrator or coincidence detector? The role of the cortical neuron revisited. Trends Neurosci 19 (4):130-7.

Lindsey, B. G., Y. M. Hernandez, K. F. Morris, and R. Shannon. 1992. Functional connectivity between brain stem midline neurons with respiratory-modulated f firing rates. J Neurophysiol 67 (4):890-904.

Lindsey, B. G., Y. M. Hernandez, K. F. Morris, R. Shannon, and G. L. Gerstein. 1992. Respiratory-related neural assemblies in the brain stem midline. J Neurophysiol 67 (4):905-22.

Lindsey, B. G., L. S. Segers, K. F. Morris, Y. M. Hernandez, S. Saporta, and R. Shannon. 1994. Distributed actions and dynamic associations in respiratory-related neuronal assemblies of the ventrolateral medulla and brain stem midline: evidence from spike train analysis. J Neurophysiol 72 (4):1830-51.

Lindsey, B. G., K. F. Morris, R. Shannon, and G. L. Gerstein. 1997. Repeated patterns of distributed synchrony in neuronal assemblies. J Neurophysiol 78 (3):1714-9.

Lindsey, B. G., and G. L. Gerstein. 2006. Two enhancements of the gravity algorithm for multiple spike train analysis. J Neurosci Methods 150 (1):116-27.

Luccioli, S., T. Kreuz, and A. Torcini. 2006. Dynamical response of the Hodgkin-Huxley model in the high-input regime. Phys Rev E Stat Nonlin Soft Matter Phys 73 (4 Pt 1):041902.

McAdams, C. J., and J. H. Maunsell. 1999. Effects of attention on orientation-tuning functions of single neurons in macaque cortical area V4. J Neurosci 19 (1):431-41.

Mohler, C. W., M. E. Goldberg, and R. H. Wurtz. 1973. Visual receptive fields of frontal eye field neurons. Brain Res 61:385-9.

Moore, G. P., Perkel, D. H., and Segundo, JP. 1966. Statistical analysis and functional interpretation of spike train data. Annu Rev Physiol 28:493-522. Moore, T. 2006. The neurobiology of visual attention: finding sources. Curr Opin Neurobiol 16 (2):159-65.

Morris, K. F., D. M. Baekey, R. Shannon, and B. G. Lindsey. 2000. Respiratory neural activity during long-term facilitation. Respir Physiol 121 (2-3):119-33.

Morris, K. F., R. Shannon, and B. G. Lindsey. 2001. Changes in cat medullary neurone firing rates and synchrony following induction of respiratory long-term facilitation. J PhyFsiol 532 (Pt 2):483-97.

Motter, B. C. 1993. Focal attention produces spatially selective processing in visual cortical areas V1, V2, and V4 in the presence of competing stimuli. J Neurophysiol 70 (3):909-19.

Mountcastle, V. B. 1997. The columnar organization of the neocortex. Brain 120 (Pt 4):701-22.

Niebur, E., C. Koch, and C. Rosin. 1993. An oscillation-based model for the neuronal basis of attention. Vision Res 33 (18):2789-802.

Niebur, E., S. S. Hsiao, and K. O. Johnson. 2002. Synchrony: a neuronal mechanism for attentional selection? Curr Opin Neurobiol 12 (2):190-4.

Perkel, D. H., G. L. Gerstein, and G. P. Moore. 1967. Neuronal spike trains and stochastic point processes. I. The single spike train. Biophys J 7 (4):391-418.

Pouget, P., E. E. Emeric, V. Stuphorn, K. Reis, and J. D. Schall. 2005. Chronometry of visual responses in frontal eye field, supplementary eye field, and anterior cingulate cortex. *J Neurophysiol* 94 (3):2086-92.

Roelfsema, P. R., V. A. Lamme, and H. Spekreijse. 2004. Synchrony and covariation of firing rates in the primary visual cortex during contour grouping. Nat Neurosci 7 (9):982-91.

Ronacher, B., A. Franz, S. Wohlgemuth, and R. M. Hennig. 2004. Variability of spike trains and the processing of temporal patterns of acoustic signals-problems, constraints, and solutions. J Comp Physiol A Neuroethol Sens Neural Behav Physiol 190 (4):257-77.

Salinas, E., and T. J. Sejnowski. 2000. Impact of correlated synaptic input on output firing rate and variability in simple neuronal models. J Neurosci 20 (16):6193-209.

Samonds, J. M., J. D. Allison, H. A. Brown, and A. B. Bonds. 2004. Cooperative synchronized assemblies enhance orientation discrimination. Proc Natl Acad Sci U S A 101 (17):6722-7.

Samonds, J. M., and A. B. Bonds. 2005. Gamma oscillation maintains stimulus structure-dependent synchronization in cat visual cortex. J Neurophysiol 93 (1):223-36.

Samonds, J. M., Z. Zhou, M. R. Bernard, and A. B. Bonds. 2006. Synchronous activity in cat visual cortex encodes collinear and cocircular contours. J Neurophysiol 95 (4):2602-16.

Sato, T., A. Murthy, K. G. Thompson, and J. D. Schall. 2001. Search efficiency but not response interference affects visual selection in frontal eye field. Neuron 30 (2):583-91.

Schall, J. D. 1991. Neuronal activity related to visually guided saccades in the

frontal eye fields of rhesus monkeys: comparison with supplementary eye fields. J Neurophysiol 66 (2):559-79.

Schall, J. D., and D. P. Hanes. 1993. Neural basis of saccade target selection in frontal eye field during visual search. Nature 366 (6454):467-9.

Schall, J. D., A. Morel, D. J. King, and J. Bullier. 1995. Topography of visual cortex connections with frontal eye field in macaque: convergence and segregation of processing streams. J Neurosci 15 (6):4464-87.

Schall, J. D., D. P. Hanes, K. G. Thompson, and D. J. King. 1995. Saccade target selection in frontal eye field of macaque. I. Visual and premovement activation. J Neurosci 15 (10):6905-18.

Schall, J. D., and K. G. Thompson. 1999. Neural selection and control of visually guided eye movements. Annu Rev Neurosci 22:241-59.

Schall, J. D. 2002. The neural selection and control of saccades by the frontal eye field. Philos Trans R Soc Lond B Biol Sci 357 (1424):1073-82.

Schiller, P. H., B. L. Finlay, and S. F. Volman. 1976. Short-term response variability of monkey striate neurons. Brain Res 105 (2):347-9.

Schmolesky, M. T., Y. Wang, D. P. Hanes, K. G. Thompson, S. Leutgeb, J. D. Schall, and A. G. Leventhal. 1998. Signal timing across the macaque visual system. J Neurophysiol 79 (6):3272-8.

Shadlen, M. N., and W. T. Newsome. 1994. Noise, neural codes and cortical organization. Curr Opin Neurobiol 4 (4):569-79.

Shadlen, M. N., and W. T. Newsome. 1998. The variable discharge of cortical neurons: implications for connectivity, computation, and information coding. J Neurosci 18 (10):3870-96.

Shadlen, M. N., and J. A. Movshon. 1999. Synchrony unbound: a critical evaluation of the temporal binding hypothesis. Neuron 24 (1):67-77, 111-25.

Shinomoto, S., and Y. Tsubo. 2001. Modeling spiking behavior of neurons with time-dependent Poisson processes. Phys Rev E Stat Nonlin Soft Matter Phys 64 (4 Pt 1):041910.

Singer, W., and C. M. Gray. 1995. Visual feature integration and the temporal correlation hypothesis. Annu Rev Neurosci 18:555-86.

Softky, W. R., and C. Koch. 1993. The highly irregular firing of cortical cells is

inconsistent with temporal integration of random EPSPs. J Neurosci 13 (1):334-50.

Softky, W. R. 1995. Simple codes versus efficient codes. Curr Opin Neurobiol 5 (2):239-47.

Steinmetz, P. N., A. Roy, P. J. Fitzgerald, S. S. Hsiao, K. O. Johnson, and E. Niebur. 2000. Attention modulates synchronized neuronal firing in primate somatosensory cortex. Nature 404 (6774):187-90.

Strangman, G. 1997. Detecting synchronous cell assemblies with limited data and overlapping assemblies. Neural Comput 9 (1):51-76.

Thompson, K. G., D. P. Hanes, N. P. Bichot, and J. D. Schall. 1996. Perceptual and motor processing stages identified in the activity of macaque frontal eye field neurons during visual search. J Neurophysiol 76 (6):4040-55.

Thompson, K. G., and N. P. Bichot. 2005. A visual salience map in the primate frontal eye field. Prog Brain Res 147:251-62.

Treisman, A. M., and G. Gelade. 1980. A feature-integration theory of attention. Cognit Psychol 12 (1):97-136.

Treisman, A., and S. Sato. 1990. Conjunction search revisited. J Exp Psychol Hum Percept Perform 16 (3):459-78.

Usrey, W. M., J. B. Reppas, and R. C. Reid. 1998. Paired-spike interactions and synaptic efficacy of retinal inputs to the thalamus. Nature 395 (6700):384-7.

Usrey, W. M., and R. C. Reid. 1999. Synchronous activity in the visual system. Annu Rev Physiol 61:435-56.

Usrey, W. M., J. B. Reppas, and R. C. Reid. 1999. Specificity and strength of retinogeniculate connections. J Neurophysiol 82 (6):3527-40.

Vogels, R., W. Spileers, and G. A. Orban. 1989. The response variability of striate cortical neurons in the behaving monkey. Exp Brain Res 77 (2):432-6.

Werner, G., and V. B. Mountcastle. 1963. The Variability of Central Neural Activity in a Sensory System, and Its Implications for the Central Reflection of Sensory Events. J Neurophysiol 26:958-77.

Wilson, M. A., and B. L. McNaughton. 1993. Dynamics of the hippocampal ensemble code for space. Science 261 (5124):1055-8.

Wolfe, J. M., K. R. Cave, and S. L. Franzel. 1989. Guided search: an alternative to the feature integration model for visual search. J Exp Psychol Hum Percept Perform 15 (3):419-33.

Wolfe, J. M., and T. S. Horowitz. 2004. What attributes guide the deployment of visual attention and how do they do it? Nat Rev Neurosci 5 (6):495-501.

Xu, N. L., C. Q. Ye, M. M. Poo, and X. H. Zhang. 2006. Coincidence detection of synaptic inputs is facilitated at the distal dendrites after long-term potentiation induction. J Neurosci 26 (11):3002-9.

Yoshimura, Y., and E. M. Callaway. 2005. Fine-scale specificity of cortical networks depends on inhibitory cell type and connectivity. Nat Neurosci 8 (11):1552-9.

Yoshimura, Y., J. L. Dantzker, and E. M. Callaway. 2005. Excitatory cortical neurons form fine-scale functional networks. Nature 433 (7028):868-73.

Yuste, R., and W. Denk. 1995. Dendritic spines as basic functional units of neuronal integration. Nature 375 (6533):682-4.

Zador, A. M., and L. E. Dobrunz. 1997. Dynamic synapses in the cortex. Neuron 19 (1):1-4.